INVESTIGATION OF THE DISTRIBUTION OF ALPHA-SMOOTH MUSCLE ACTIN POSITIVE CELLS AT COLLECTOR CHANNEL OSTIA IN NORMAL HUMAN EYES

A thesis presented to the graduate faculty of
New England College of Optometry in partial fulfillment
of the requirements for the degree of Master of Science

Kevin C. H. Chan

April, 2013

© Kevin C. H. Chan
All rights reserved

The author hereby grants New England College of Optometry permission to reproduce and to distribute publicly paper and electronic copies of the thesis document in whole or in part.

INVESTIGATION OF THE DISTRIBUTION OF ALPHA-SMOOTH MUSCLE ACTIN POSITIVE CELLS AT COLLECTOR CHANNEL OSTIA IN NORMAL HUMAN EYES

Kevin C. H. Chan

This manuscript has been read and accepted by the
Thesis Committee in satisfaction of the
thesis requirement for the degree of Master of Science

4-22-13
Date

Haiyan Gong, Ph.D.
Graduate Faculty Advisor

Nancy J. Coletta, O.D., Ph.D.
Thesis Committee Member

Barry M. Fisch, O.D.
Thesis Committee Member

Andrew Taylor, Ph.D.
Thesis Committee Member

5-16-13
Date

Nancy J. Coletta, O.D., Ph.D.
Director of Graduate Studies

New England College of Optometry

INVESTIGATION OF THE DISTRIBUTION OF ALPHA-SMOOTH MUSCLE ACTIN POSITIVE CELLS AT COLLECTOR CHANNEL OSTIA IN NORMAL HUMAN EYES

Kevin C.H. Chan

New England College of Optometry, 2013

ABSTRACT

Introduction: Intraocular pressure (IOP) is one the major risk factors for the development of primary open angle glaucoma (POAG). However, its progression can occur under normotensive or elevated IOP. Previous studies reported that 51% outflow resistance under normal IOP still existed even after 360-degree trabeculotomy, suggestive of residual outflow resistance could be present at distal outflow region. Smooth muscle-like cell have been found at distal outflow region near collector channel (CC) ostia, yet its morphological and functional characteristics remain unknown in regulation of outflow resistance. The goals of our study are: 1) To reconstruct distribution patterns of collector channels in human eyes, using frontal and circumferential sections; 2) To identify α-smooth muscle actin positive cells near CC ostia in both radial and frontal orientations using immunohistochemistry.

Methods: Twelve enucleated human eyes were dissected into radial (n = 6), frontal (n=3), circumferential (n=3) orientation. After a series of paraffinization, samples were sectioned and stained with Hemotoxylin & Eosin (H&E) and Trichrome solution to identify the CC ostia and smooth muscle-like cells near CC ostia. Samples were imaged in light microscopy

for morphological analysis. Indirect immunohistochemistry and fluorescence microscopy imaging were performed to identify α-smooth muscle actin positive cells near CC ostia.

Results: Thirteen patent CCs were found in frontal orientation. The majority were located at inferior nasal (61.5%), followed by superior temporal and mid-nasal quadrants (30.8%). Number of CC ostia at inferior nasal quadrant was shown statistically higher than other three quadrants: superior temporal, inferior temporal, and superior nasal ($p<0.001$). Trichrome-stained smooth muscle-like cells were identified at the junction of CC ostia, yet its spatial distribution is highly variable. Two distinct types of CC ostia were found. Presence of smooth muscle-like cells was not associated with any morphological variations of CC ostia. Positive immunofluorescence staining indicating α-smooth muscle actin was revealed with statistical significance in radial samples only ($p<0.0001$). Fluorescence pattern was mostly found at outer wall of SC with sparse distribution in some CC ostia, but not others, in both radial and frontal sections. The overall pattern of immunofluorescence lacks consistency regardless of CC orifice size or patency.

Conclusions: Despite the lack of morphological association between distribution of α-smooth muscle actin and specific morphology of CC ostia, contractility of α-smooth muscle actin may suggest its potential role in governing collector channel ostia, and thus regulating outflow resistance.

ACKNOWLEDGEMENTS

I would like to express the deepest gratitude and appreciation to my thesis advisor, Dr. Haiyan Gong, Associate Professor of Ophthalmology and Anatomy and Neurobiology at Boston University. This thesis would not have been possible without Dr. Gong's continual guidance and unfailing support throughout these past 4 years. Through her tireless effort in editing the thesis draft to the completion and dedicated passion in fostering students in academic research, I am fortunate to have undergone the mentorship of Dr. Gong. Despite the frustration in experimental failures and countless hours working in the laboratory after school at nights and weekends, her patience and inspiration has truly been a momentum for me to overcome all the laboratory and technical obstacles and, finally, to the completion of this research work.

I would also like to thank my thesis committee members, Drs. Nancy Coletta, Andrew Taylor, Barry Fisch, for their valuable time in reading my thesis and offering new insights and advice for my research work.

In addition, I sincerely would like to thank the laboratory colleagues who have offered me technical support and developed a great platform and atmosphere for academic discussion. I thank Mr. Elliot Cha, laboratory lead assistant, for his technical guidance and demonstration in experimental setups in preparation of histological specimen and fluorescence microscopy. I am grateful for having Ms. Rozanne Richman for her excellent technical assistance, even after her retirement. I also thank Mr. Adrian Cann, a senior undergraduate biology student

doing the pilot morphology study of collector channels in mice model, for his technical assistance in using ImageJ and his ingenuity in stimulating my work. My appreciation is also for Ms. Rui Jin (Sherry) for her assistance in tissue sectioning.

Lastly, yet not the least, I would like to thank my family for giving me tremendous mental support and believing in me despite I have constantly been frustrated and self-doubtful of accomplishing this insurmountable goal. Thank you Lord for the unfailing love in guiding and guidance through the difficult moments and molding me to become the person I am today.

Table of Contents

Abstract iii

Acknowledgement v

Introduction 1

2. Methodology

2.1. Preparation of Frontal Reconstruction of Collector Channel Ostia

2.1.1. Sampling 6

2.1.2. Tissue embedding and sectioning 7

2.1.3. Hematoxylin and Eosin (H&E) & Masson's Trichrome Staining 8

2.1.4. Light Microscopy 10

2.2. Immunofluorescence Analysis of Alpha-Smooth Muscle Actin at regions of Collector Channel Ostia

2.2.1. Immunofluorescence Staining of Collector Channel Ostia 10

2.2.2. Fluorescence Microscopy Imaging 12

2.2.3. Statistical Analyses 13

3. Results

3.1. Global Reconstruction and Distribution of Collector Channel Ostia in Frontal Orientation 13

3.2. Interconnectivity of Inter-Collector Channels and Morphological Types of Collector Channel Ostia 17

3.3. Immunofluorescence Staining of Alpha-Smooth Muscle Actin at Distal Outflow Regions 19

4. Discussion

4.1. Morphological and Mechanical Observation of Collector Channel Ostia and Distribution Pattern of Alpha-Smooth Muscle Actin 22

4.2. Distribution Patterns of Collector Channels & Factors of Variability 26

4.3. Factors governing Antibody Immunofluorescence 28

4.4. Roles of Transforming Growth Factor Beta-2 (TGF-β2) in Alpha-Smooth Muscle Actin Cells 30

4.5. Patterns of Interconnectivity between Schlemm's canal and Supraciliary Space 33

5. Direction of Future Studies

5.1. Identify Collector Channel Ostia using Thinner Sections 35

5.2. Reexamination of Immunostaining of Alpha-Smooth Muscle Actin and Determine its Role in Regulating Aqueous Outflow 36

5.3. Role comparison of Alpha-Smooth Muscle Actin between Normal and POAG Human Eyes 36

6. Conclusion 37

7. Bibliography 38

List of Tables and Figures

i.	Table 1	Quadrant distribution of distal collector channels of human normal eyes in frontal sections	46
ii.	Figure 1	Dissection techniques of radial, frontal, and circumferential views	47
iii.	Figure 2	Spatial comparison of collector channel ostia between nasal and temporal quadrants in frontal sections	48
iv.	Figure 3	Spatial comparison of collector channel ostia between superior and inferior quadrants in frontal sections	49
v.	Figure 4	Comparison of Hematoxylin-Eosin (H&E) and Trichrome-Masson staining patterns in frontal orientation	50
vi.	Figure 5	Interconnectivity of adjacent collector channel and episcleral venous plexus stained with Trichrome-Masson stain	51
vii.	Figure 6	Morphological types of collector channel ostia observed in frontal perspective	52
viii.	Figure 7	Comparison of interconnectivity between collector channels and supraciliary space in serial radial sections between pre- and post-Trichrome-Masson staining	53
ix.	Figure 8	Indirect immunofluorescence staining for α-smooth muscle actin with monoclonal anti-mouse primary and secondary antibodies	54
x.	Figure 9	Distribution of immunofluorescence at regions of collector channel ostia between radial and frontal views	55 – 56
xi.	Figure 10	Quantitative comparison of immunofluorescence at regions of collector channel ostia between radial and frontal views	57

Introduction

Primary open-angle glaucoma (POAG) is generally described as progressive optic neuropathy characterized by structural damage to the optic nerve head, open anterior chamber angle, and glaucomatous visual field defect, with no other underlying disease. Glaucoma (both open-angle and angle-closure glaucoma) is the second leading cause of blindness worldwide and it is predicted to increase up to 80 million people worldwide by 2020 (Quigley et al, 2006). In particular, POAG is considered the leading cause of irreversible blindness in African Americans (Sommer et al., 1991). Some common risk factors have been identified for POAG, including aging, family history, African origin, elevated intraocular pressure. However, there is yet no specific diagnostic criterion that accurately defines POAG. Elevated intraocular pressure (IOP) is considered one of the major risk factors for the development and progression of POAG. However, elevated IOP is not present in all forms of glaucoma and it lacks consensus as of which specific IOP value should be deemed as 'normotensive' or 'glaucomatous'. For example, normal tension glaucoma (NTG) develops as optic neuropathy with similar characteristics of POAG, yet in presence of lower IOP level. There has been no single cutoff level of IOP at which POAG can always be claimed to develop or not (Sommer et al., 1989). Despite efforts of studying the relationship of IOP and glaucomatous optic neuropathy, it lacks consistency based on various population-based studies (Sommer et al., 1991; Mitchell et al., 1996; Leske et al., 1994; Quigley et al., 2001; Klein et al., 1992). In general, intraocular pressure (IOP) is regulated by aqueous outflow through trabecular meshwork (TM), Schlemm's canal (SC), collector channels (CC), through which outflow ultimately exits via episcleral venous plexus (Grant, 1951). It was

postulated that elevated IOP mainly resulted from increased outflow resistance (Leber, 1873; Grant, 1958). Outflow resistance via TM outflow pathway generally increases with age (Worley and Grimmer-Somers, 2011; Gabelt and Kaufman, 2005; Ethier et al., 1998) and in POAG. Previous experimental flow studies suggested that the primary site of outflow resistance is likely to be the greatest at juxtacanalicular connective tissues (JCT) region (Mäepea, O. & Bill, A, 1992; Johnson and Kamm, 1992; Ethier, 2002; Johnson, 2006) Based on the quantitative study which measured the point at which the reduction of pressure occurred using a micropressure sensor through the inner wall of SC and into the trabecular meshwork, the greatest pressure drop was found occurred within 14 μm of the inner wall of SC, a position that corresponds to a point within the JCT (Mäepea, O. & Bill, A, 1992). Despite years of investigation, however, the exact source and mechanism of outflow resistance still remains controversial. Recently, structural and morphological changes of anterior chamber structures in dependence of IOP changes have been reported (Zhu el al, ARVO abstract 2007; Battista et al, 2008). Acute elevation of IOP in bovine eyes displayed reduction in outflow facility, which was also associated with the collapse of aqueous plexus (bovine equivalent of SC in humans) as well as increased number of herniations of the TM into the CC ostia. Several other studies suggested that increased outflow resistance is associated with increased extracellular matrix (ECM) and the presence of matricellular proteins, thrombospondin-1 (Flϋgel-Koch et al., 2004), which resulted in dynamic turnover and remodeling processes (Acott and Kelley, 2008; Keller et al., 2009). In addition, a recent study using laser-induced glaucomatous cynomolgous monkey eyes has found that, under chronic elevation of IOP, decreased outflow facility was associated with lower percentage of effective filtration length

(PEFL; ratio between the length of inner wall of SC exhibiting tracer labeling and the total length of inner wall (Zhang et al., 2009). Previous studies have shown that after complete (12 clock-hour) trabeculotomy, only 49% of outflow resistance was eliminated at normal IOP in enucleated human eyes (7 mm Hg) and 29% of outflow resistance still remains at higher IOP (25 mm Hg) (Rosenquist et al., 1989; Grant WM. 1963). It suggested that the change in outflow resistance with increasing IOP is likely associated with pressure-dependent changes in the TM and SC. In calculation of hydraulic conductivity, Bill and Svedbergh (1972) also examined the outflow resistance generated by inner wall pores of SC and indicated that the inner wall endothelium could not generate more than 10% of the total outflow resistance at TM region. It further suggests that additional sources of resistance distal to the inner wall of SC likely exist and may contribute to increased outflow resistance with increasing IOP. However, the mechanism of how distal outflow resistance was generated and regulated is still unknown.

To better understand the functional morphology of distal outflow areas, growing interest has been developed to investigate the influence of cellular contractility at this region. The control of outflow facility has previously been linked to the active contractility of trabecular meshwork containing myofibroblasts, which resembled “smooth muscle-like” cells in rat (Tsukahara, 1978), rabbit (Knepper et al., 1974; Sakimoto and Samejima, 1977a,b), and pig-tailed Macaque (McMenamin and Lee, 1982), respectively. A specific isoform of actin filament, known as α-smooth muscle actin (α-SM actin), shows specific expression in vascular smooth muscle cells and myofibroblasts. It was found to be localized at the region

of outer wall of Schlemm's canal, along with some scattered cells being expressed in collector channels in bovine and human samples (Gipson and Anderson, 1979; Grierson et al., 1986; Iwamoto & Tamura, 1988; Coronero et al., 1991; de Kater et al., 1990, 1992; Flügel et al., 1991). While its presence has been evident in ciliary muscles, trabecular meshwork, and Schlemm's canal regions, to our knowledge, little has been known or studied regarding the anatomy, morphology, and functional variations of collector channels. Only few studies examining α-SM actin were exclusively done at collector channel ostia in normal albino rabbits and human eyes (Sakimoto et al., 1977a & b; De Kater et al., 1990 & 1992). While the latter study of De Kater et al. (1992) had identified the heterogeneity of α-SM actin and F-actin at the distal components of outflow pathway using immunohistochemical techniques, however, samples were compared solely in radial orientation, which limited the dimension into a single quadrant of outflow pathway. Moreover, it also lacked spatial comparison of α-SM actin distribution as well as its immunofluorescence expression among different quadrants. Interestingly, Battista et al. (2008) and Hann et al. (2009) have recently brought insights that fluid outflow was preferentially distributed under collector channel ostia of bovine and human eyes, respectively. It has been demonstrated that the aqueous humor outflow flowing through the trabecular meshwork is not uniform, but segmental. More outflow, demonstrated by tracer, was found in the trabecular meshwork near the collector channels, yet not in all collector channel ostia. In addition, increased outflow pattern was found to be localized in the inferior and nasal quadrants. The underlying mechanism remains elusive whether the distribution of α-SM actin is likely to play a role in regulating the distal outflow pattern, which, in turn, may contribute to the segmental flow pattern. It is

hypothesized that the distribution of α-SM actin is not uniform, and its cellular contractile properties is likely to be involved in governing distal aqueous outflow pattern. In essence, there are mainly two objectives in this study. First, we attempt to reconstruct a structural model of spatial distribution patterns of collector channels in frontal perspective using normal, non-glaucomatous, human eyes obtained from the Eye bank. Second, we attempt to identify α-smooth muscle actin positive cells near collector channel ostia in both radial and frontal orientations using immunofluorescence techniques.

In addition, as inspired by earlier studies of episcleral arteriovenous anastomoses (AVA) (Funk et al, 1996; Funk & Rohen, 1996; Selbach et al., 1998), AVA were found to be proximally localized at collector channel ostia and that arterial transport via AVA is directly linked to episcleral venous plexus, from which episcleral venous pressure (EVP) was shown to be associated with IOP. Since anastomoses had been established between the neighboring structures of different origins, it may not be surprising that interconnectivity could also exist within adjacent collector channels as well as within the routes of collector channels and supraciliary space in the outflow pathway. The potential interconnectivity in radial orientation, as well as among adjacent collector channels in frontal orientation were also examined in this study.

2. Methods

2.1 Preparation of Frontal Reconstruction of Collector Channel ostia in normal human eyes stained with Hematoxylin and Trichrome-Masson solution

2.1.1. Sampling

A total of twelve enucleated normal human eyes were obtained from the National Disease Research Interchange (Philadelphia, PA) within 24 hours postmortem during the period of 1995 to 2011. Samples were divided into three groups with particular orientations: radial (n=6), frontal (n=3), and circumferential (n=3) views, respectively. Eyes were grossly examined under dissecting microscope to ensure no discernible structural alternation or damage, particularly at the angle of the anterior chamber. Those with prior ocular injury or surgery were excluded from the study. Eyes were fixed in formalin solution (pH 7.4) and refrigerated until further processing. Fixed eyes were first dissected into halves along the equator of the globe. Vitreous and lens were carefully removed. Wedges of tissues (grossly 1.0-1.5 mm in thickness) from the anterior portions of the globe were dissected and classified as radial sections. With the technical assistance by the senior technician, Rozanne Richman, tissue samples from the whole eye specimen were also dissected. Radial section was described as an orientation perpendicular to limbus, which represented a small cross-sectional view of a collection of anatomical structures with limited proximity to the collector channel ostia. Frontal section, on the other hand, was described as the plane of orientation

tangential to limbus, which allows broader perspective of collector channel ostia and other distal outflow structures (Fig. 1).

2.1.2. Tissue embedding and sectioning

In process of paraffinization, all the fixed tissues were rinsed with phosphate buffered saline to remove paraformaldehyde in the fixative. Tissues were dehydrated with an ascending series of alcohol (70%, 95%, and 100% for 30 minutes each and infiltrated with xylene for 1 hour, followed by a second infiltration for 30 minutes at room temperature. Tissues were then permeabilized in mixture of xylene and paraffin (1:1 volume ratio) overnight in oven at 60°C. After removal from xylene-paraffin mixture the next day, tissues were incubated in paraffin for 2 hours at 60 degrees. Later, tissues were embedded in paraffin wax-filled lead block. Preheated forceps was used to orient tissues in a correct orientation, parallel to the base of lead block. Tissue block was placed in ice bath for 20 minutes until hardened for sectioning.

Tissue blocks to be sectioned were securely placed on the microtome and a fresh microtome blade was aligned at an angle of approximately 4-6° to the block. The cutting dial was set to be 6 µm per section. The first few paraffin ribbons were discarded until smooth, uniform ribbon pieces were generated. Three ribbon pieces of tissue were serially cut each time and they were carefully transferred with a fine, unwetted paint brush onto the surface of water bath coated with gelatin at 37°C. Gelatin solution was gently stirred until dissolved which

was used to minimize wrinkling of the sectioned tissues. Floating sections were carefully picked up by sliding them onto the surface of glass slides obliquely. Glass slides were then placed on top of the heater at 37°C overnight until sectioned tissues were dry.

2.1.3. Hematoxylin and Eosin (H&E) & Masson's Trichrome staining

Two staining methods have been used for control and sample comparisons in this study. Samples of two human eyes used for controls were all previously prepared in frontal orientation and stained with Hematoxylin and eosin (H&E) by a senior technician. Three samples in the same frontal orientation in presence of patent collector channel ostia were stained with Masson's Trichrome. No sample in radial orientation was stained with H&E protocol except the sections for potential antero-posterior interconnectivity in this study. H&E staining has long been used routinely in histopathological analysis to identify nuclear, cytoplasmic, and other cellular features. Hematoxylin reacts as a basic dye which stains nucleic acids in deep blue-purple color whereas eosin is an acidophilic dye which reacts non-specifically with cytoplasm and collagen matrix in pink color (Fischer et al. 2008). The intensity of H&E stain is dependent on the affinity of eosin and hematoxylin toward positively and negatively charged molecules, respectively. On the other hand, Masson's Trichrome is a tri-color staining protocol primarily intended for histological observation of smooth muscle-like tissue and collagenous connective tissue fibers.

Upon sectioning, all tissue sectionson glass slides were first deparaffinized with xylene for 5 minutes in 2 cycles, followed by a series of rehydration process with 100%, 95% ethanol and

deionized water. Staining process first began with Bouin's solution (Sigma catalog #HT10-1) which was preheated at 60°C for 15 minutes. Tissue slides were submerged and stained with Bouin's solution for 5 minutes. Slides were then washed under tap water and rinsed in deionized water for 5-10 minutes until yellow color was rinsed off from the slides. After rinsing, tissue slides were stained with Weigert's Iron Hematoxylin solution (Catalog #HT10-79) for 5 minutes. Hematoxylin solution was made by 1:1 mixture of Solution A (Catalog #HT10-7; 1% Hematoxylin in 95% ethanol) and Solution B (Catalog #HT10-9; 1.2% (w/v) Ferric Chloride and 1% (v/v) Acetic Acid in distilled water). Slides were then washed and rinsed with deionized water for 5-10 minutes. Later, tissue slides were stained with Biebrich Scarlet-Acid Fuchsin (Catalog #HT15-1) for 5 minutes, followed by rinsing with deionized water for 10-15 minutes or longer due to dark staining property. Tissue slides were subsequently placed in Phosphomolybdic/ Phosphotungstic Acid Solution for 5 minutes. It was prepared by mixture of Phsophomolybdic Acid Solution (Catalog #HT15-3), Phosphotungstic Acid Solution (Catalog #HT15-2), and deionized water in 10:10:20 volumetric ratio. The solution was discarded after each usage. Tissue sections were subsequently stained with Aniline Blue Solution (Catalog #HT15-4) for 5 minutes, followed by brief rinse in deionized water. To render delicacy and transparency of the shades of color, 1% acetic acid solution was used for the slides for 3-5 minutes. After a brief rinsing, sections were prepared for dehydration with 95%, 100%, and xylene for 5 minutes each. Tissue slides were then mounted with permount gel by gently inserting coverslips obliquely to allow full coverage of tissues and minimize bubbling effect. Specimens were placed at room temperature for drying overnight.

2.1.4. Light Microscopy

To appreciate the presence and overall pattern of collector channels in a 360-degree perspective, three tissue slides were initially prepared and pre-dissected as the whole anterior segment sections by the senior technician, two of which in good Trichrome staining quality. Subsequently, they were sent to Alcon Research Institute (Fort Worth, TX) at which tissue slides were scanned and captured in high capacity facility using ScanScope (v11.0.02.725; Aperio ePathology Solutions). Panoramic views were captured at magnification ranges up to 20X to analyze the morphological variations of Schlemm's canals and collector channels. In particular, clear and open structures were further magnified and imaged in snapshots according to their clock-hour positions. Samples numbered in sequence were arranged on the basis of order of sectioning anteriorly to posteriorly. They were compared for the morphological variations of positive staining of smooth muscle-like cells in frontal sections (See section 2.2 below).

2.2. Immunofluorescence Analysis of α-smooth muscle actin at regions of collector channel ostia

2.2.1. . Immunofluorescence staining of collector channel ostia

Radial sections from six eyes and frontal sections from three eyes were examined and compared for the immunofluorescence staining pattern. The radial sections from two eyes

were later discarded because of structural damage and discontinuity after processing. Tissue slides were first prepared for dehydration process by xylene, along with serial steps of alcohol, as previously described. After dehydration, tissues were briefly rinsed with PBS. Tissue sections were aspirated to remove PBS and subsequently submerged into microwave-heated 10mM 0.05% citrate buffer solution (pH 6.0; Fisher Scientific, Fair Lawn, NJ). The solution resulted from mixture of 1.92 g citric acid with 1000 ml distilled water. Solution was mixed to dissolve until pH reached 6.0 with acid-base titration accordingly. Modified protocol was attempted in which citrate buffer solution was preheated in microwave for 45-60 seconds prior to submerging tissue slides into the buffer solution. It was intended to avoid detachment of tissues from glass slides during heating process. Tissue detachment was possibly due to insufficient dehydration of tissues. Previous studies showed that citrate buffer treatment was beneficial in immunohistochemical detection of androgen receptor in formalin-fixed paraffin sections (Shi et al. 1993; Kanai et al. 1998). Utility of microwave heating further enhanced the effectiveness of antigen retrieval in formalin-sensitive epitopes (Pellicer et al. 1994; Brown et al. 1995). After tissue slides were cooled down at room temperature, 0.01% triton X-100 solution (Sigma T8787, St. Louis, MO; dilution 1:100), was used to permeabilize the cell membrane and reduce surface tension during immunostaining. Tissues were then treated with 1% (w/v) bovine serum albumin (BSA) in DPBS for 1 hour (5% BSA, Sigma A-9647; dilution 1:5) to block non-specific binding sites. The sections were then incubated with primary antibody, monoclonal mouse anti-α smooth muscle actin antibody ($IgG_{2\alpha}$) (Sigma A2547; dilution 1:400) overnight at 4°C in PBS containing 1% BSA and 0.001% Triton X-100. Negative control was treated by PBS in substitution of the primary

antibody, which was then treated with the mouse IgG secondary antibody. PBS elicited no immunochemical reactivity with the secondary antibody and, therefore, no immunofluorescence was expected to be seen. The samples of interest were washed 3 times with PBS and incubated with the secondary antibody (Alexa Fluor 488 goat anti-mouse IgG (H+L, Invitrogen A11001; dilution 1:500) for 2 hours at room temperature. The sections were again washed with PBS 3 times for 5 minutes each. Vectashield mounting medium (4'-6-Diamidino-2-phenylindole, DAPI; Life Technologies, Carlsbad, CA) was then added onto tissue sections for nuclei staining by forming fluorescent complexes with AT regions of double-stranded DNA. Cover glass slides were placed on top of tissues obliquely to avoid bubble formation. Aluminum foils were used over the glass slides to minimize photochemical reactions.

2.2.2.. Fluorescence Microscopy Imaging

Tissue sections processed with immunohistochemistry were examined by fluorescence microscopy. The sections were examined with fluorescence microscopy (FSX-100, Olympus, Tokyo, Japan) using 10x, 20x, 40x, up to 60x, objective at specific exposure times relative to the magnitude of magnification. Images were captured at the locations at which areas of collector channel ostia were evident, patent, as well as the number of collector channels was quantified, regardless of the presence or absence of immunofluorescence staining. Samples were observed independently of quadrant positions in order to minimize biased collection of data.

2.2.3. Statistical Analyses

Unpaired two-tailed student's t-test was applied for the analysis of statistical significance between the means of the two sub-regions within each quadrant (E.g. statistical difference between superior and inferior region within the nasal quadrant). One-way analysis of variance (ANOVA) was used to analyze the statistical difference among the groups in all three quadrants (E.g. difference of the inferior region among nasal, midsection, and temporal quadrants). The required significance level is 0.05.

3. Results

3.1. Global Reconstruction and Distribution of Collector Channel Ostia in Frontal Orientation

Dissections of radial, frontal, and circumferential views of normal human eyes were depicted in Figure 1. Demographics and distributions of collector channels observed in frontal perspective were summarized in Table 1. Among the three frontal samples, a round-up total of 13 visible collector channels were observed. The collector channels were found to be in non-uniform distribution circumferentially, most of which were located at inferior nasal (61.5%), followed by superior temporal and mid nasal quadrants (30.8%). The least amount of collector channels present in this study was found to localize at superior and inferior positions combined (7.7%). In perspective of meridians only, patent collector channels were

shown to be present more on the horizontal meridian (28.6%), defined as 3 and 9 o'clock positions, than on the vertical meridian (7.1%), defined as 6 and 12 o'clock positions. For the horizontal meridian only, collector channels were shown to be present more on 3 o'clock position (17.9%) than its 9 o'clock counterpart (10.7%). However, the absolute numbers of patent collector channels were shown to be equal between 12 o'clock position (3.6%) and 6 o'clock position (3.6%).

In perspective of nasal region only (bars in blue), the distribution of collector channel ostia among the superior, midsection, and inferior quadrants, collector channel ostia were predominantly localized at inferior quadrant with statistically significance compared to two other quadrants (inferiorly nasal (IN) = 9.0; midsection nasal (MN) = 3.0; superiorly nasal (SN) = 1.7; labeled as +++; One-way ANOVA, $p < 0.001$) (Fig. 2). However, collector channel ostia located at temporal regions among the same three quadrants did not show any statistical significance (bars in red; $p = 0.569$). Within the inferior quadrant independently, collector channel ostia were shown to outnumber at nasal than temporal quadrant (inferiorly nasal (IN) = 9.0; inferiorly temporal (IT) = 3.3), and the spatial difference between the two regions was shown to be statistically significant (labeled as ***; student T-test, $p < 0.01$) (Fig. 2). No other statistical significance was found between nasal and temporal regions within superior quadrant ($p = 0.561$) and midsection ($p = 0.184$), respectively. Meanwhile, in comparison of spatial distribution of collector channel ostia between superior and inferior quadrants only, interesting results were found in Fig. 3. Looking at the inferior region among nasal, midsection, and temporal quadrants (bars in green), collector channel ostia were

mostly distributed at nasal quadrant, and the difference among the three quadrants was statistically significant (nasally inferior (NI) = 11.3; midsection inferior (MI) = 1.3; temporally inferior (TI) = 3.3; labeled as +++; one-way ANOVA, $p < 0.0001$). In perspective of superior region among these three same quadrants (bars in orange), collector channel ostia were more likely to be found in temporal quadrant. Meanwhile, the differences among temporal, midsection, and nasal quadrants were also shown to be statistically significant despite the difference appeared to be less obvious (temporally superior (TS) = 6.0; midsection superior (MS) = 1.0; nasally superior (NS) = 3.0; labeled as ▲ ; $p < 0.05$). Within the nasal quadrant independently, the distribution of collector channel ostia were statistically greater at inferior than superior regions (nasally inferior (NI) = 11.3; nasally superior (NS) = 3.0; labeled as ***; student T-test, $p < 0.005$). No other statistical significance was found between superior and inferior regions within midsection ($p = 0.374$) or temporal quadrant ($p = 0.14$), respectively.

Despite collector channels were shown to have some preferential localization patterns with statistical significance, particularly in inferior and nasal region individually, as well as in combination of both regions, it might not invariably reflect the true spatial representation of collector channel ostia in a larger scale since the sample size used was small in this study. To better evaluate the statistical significance, it may warrant a larger sample size in future in order to differentiate how collector channels are specifically localized in a quantitative manner.

In comparison of Trichrome with Hematoxylin-eosin stained samples shown in Fig. 4, all the three samples in frontal orientation demonstrated distinctly positive red staining for smooth muscle-like cells, despite the few batches in each sample that represented one of the many cross-sectional slides were either out of focus or in faded stain color. In general, smooth muscle-like cells stained in Trichrome red were shown evident at the outer wall of Schlemm's canals as well as the "bottleneck" opening region of collector channels, from which it displayed tendency to further extended to the distal collector channels. No Trichrome-stained samples in radial orientation was compared or shown in our study because our interest and attempt is mainly to localize the distribution of collector channel ostia in frontal perspective. Also, it was known that such cutting technique has already been utilized in studies by De Kater el. (1990, 1992) and the results showing the presence of smooth muscle-like cells observed in radial orientation in human eyes had been published. In this study, almost all tissue slides within each sample were Trichrome-stained and arranged sequentially in its best effort such that collector channels shown as partially closed or incomplete were examined in the sequence of how the tissue slides were sectioned as a whole. In other words, the red stain indicating smooth muscle-like cell type that contoured from partial opening to complete patency of distal collector channels were traced and taken into consideration in order to minimize the possible overlooked structures. Nevertheless, it was inevitably difficult to capture the images from all sample slides sequentially because of sample wrinkling or scratching during tissue processing.

The absolute number of stained collector channels at inferior nasal quadrant was observed to

be almost 4-fold greater as compared to the same quadrant in unstained samples (12 in stained vs. 3 in unstained $\pm$ 6.36). However, after taking all other quadrants into consideration, the average number of collector channels found in the stained samples was not shown to be statistically different from that in the unstained samples (3 channels $\pm$ 3.85 vs. 1.63 channels $\pm$ 1.30; student t-test; $p = 0.129$).

3.2. Interconnectivity of Inter-Collector Channels and Morphological Types of Collector Channel Ostia

Potential structural interconnections between adjacent collector channels and/or episcleral venous plexus in circumferential and frontal section were demonstrated in Fig. 5. Two of the three samples showed evidence of potential interconnections between adjacent collector channels. In panoramic view of whole eye specimen shown in Fig. 5a, interconnectivity of CC ostia and distal episcleral venous plexus appeared to localize at inferior nasal quadrant of the left eye. Yet, it represents one section only and it might not necessarily reflect the overall distribution of potential interconnections between CC ostia and distal episcleral venous plexus. More structural interconnections are likely to be seen if more sections were cut and observed. During the technique of serial sectioning, however, the task can be challenging to reveal well-defined representations of interconnections between distal outflow structures at all levels. It is mainly because the structures can be variable depending on the levels of serial sections, or how much deviation the section was cut initially. Stemming from Schlemm's canals, three patent collector channels in frontal orientation were shown to have long,

continuous extension in conjunction with episcleral venous plexus as a loop circuit. It was shown with Trichrome red staining lining along inner and outer walls collector channels in uniform distribution (Fig. 5c). Batches within each sample, however, displayed inconsistent and incomplete collector channels, at which stronger staining intensity of red Trichrome lined along its outer wall in discontinuous pattern. Eventually, its extension was stalled to link with adjacent channels (Fig. 5d). Such trend of collector channels observed among the small sample size were shown to be localized at inferior temporal quadrants in two right eye samples and at inferior nasal quadrants in four left eye samples, respectively. They are likely to suggest that the potential interconnectivity may occur between the outer wall of SC and episcleral venous plexus, rather than within neighboring collector channels.

Two different types of collector channel ostia were identified and shown in Fig. 6. Slides of few distinctive representations, yet not inclusively found in all samples, includes: 1) Oblique extension of CC ostia from the bottleneck region of Schlemm's canal in unidirectional manner (Fig. 6a); 2) bidirectional budding of CC ostia in Y-shaped bifurcation (Fig. 6b). Among the two morphological variations of distal CC ostia, Trichrome staining patterns and intensity were shown to be highly variable. The extent and intensity of Trichrome staining were shown to be more prominent at the type of unidirectional CC ostia, adjacent to the bottleneck opening region between Schlemm's canal and CC ostia, than at the distal tips of CC ostia after bifurcation. However, due to the lack of staining specificity for smooth muscle subtypes by Trichrome stain as well as the small sample size, in this study it cannot conclusively identify if smooth muscle-like cells are preferentially present with specific

morphology of CC ostia. Given our preliminary observation of morphological variations of CC ostia, more future work is warranted to determine if α-smooth muscle actin were indeed associated with any specific morphological type of CC ostia.

Moreover, in view of radial orientation, morphological variations of collector channels were observed and compared before and after Trichrome staining procedure (Fig. 7). Trichrome staining in radial orientation was utilized only in purpose of comparing possible structural variations and connectivity among collector channels in this study. In a series of 18 radial sections within one sample (only 4 major serial sections were displayed in Fig. 7), collector channels budding out from Schlemm's canals in all pre-Trichrome stained samples were shown to demonstrate traces of connectivity between SC and supraciliary space. Routes of collector channels were varied from Y-shaped anterior-to-posterior bifurcation to oval-shaped sliding pattern to supracilary space. Post-Trichrome stained samples, however, did not reveal corresponding pre-Trichrome findings in this study. Inconsistent staining patterns were found in which 22.2% (4 of 18) of radially sectioned samples lacked labeled staining for smooth muscles and almost all samples were presented with structural discontinuity of collector channels.

3.3. Immunofluorescence staining of α-smooth muscle actin at distal outflow regions

Immunofluorescence staining was demonstrated in various types of ocular tissues, as shown in Figure 8. Structures containing α-SM actin were evident in iris blood vessels and dilator

muscle (Fig. 8A and B), ciliary muscle in the ciliary body (Fig. 8C and D), and smooth muscle fibers surrounding episcleral vein (Fig. 8E and F). The signals were elicited for the immunospecific binding between monoclonal anti-mouse primary antibody (IgG2α) and secondary antibodies (Alexa Fluor 488 goat anti-mouse IgG (H+L). The positive binding confirmed that existing α-smooth muscle actin in those particular regions.

In observation of morphological manifestations of immunofluorescence-stained samples, the distribution patterns of immunofluorescence depicting α-smooth muscle actin at regions of CC ostia were illustrated in Fig. 9. Structures in radial view displayed as continuous, filamentous, and pyramidal pattern were mostly localized at the outer wall of Schlemm's canals. Few sparse signals in neighbor with collector channel ostia were found (Fig. 9D & E). On the other hand, in view of frontal orientation, the intensity of immunofluorescence signal appeared to be brighter at the junction of outer wall of SC before bifurcation than the distal vicinity of collector channels (Fig. 9G). Moreover, the signals were more likely revealed as 'punctate', rather than elongated or filamentous, pattern of α-smooth muscle actin. Other variable patterns of immunofluorescence included small, discrete 'micro-punctate' appearance that were selectively localized at the distal tip, rather than confluent 'satellite' appearance surrounding the entire collector channel budding out from outer wall of SC (Fig. 9H). However, no significant evidence or consistent pattern of immunofluorescence was found which could invariably suggest that α-smooth muscle actin cell type fully in surrounding of CC ostia, regardless of the sizes of orifices or the patency of collector channels.

Immunofluorescence labeling with positive signals in vicinity of collector channel regions were later compared between radial and frontal orientation in Fig. 10. Presence of immunofluorescence corresponding to α-SM actin was found to be variable within the same region between radial and frontal sections. In view of radially sectioned samples, positive immunofluorescence signal was shown to be significantly greater (3.91 $\pm$ 1.37 collector channels) than those without immunofluorescence staining (0.45 $\pm$ 0.69 collector channels; $p < 0.0001$). Interestingly, the amount of immunofluorescence signals depicting the same structure in frontal sections were found to be more sparse and irregular in the samples with positively-stained immunofluorescence (3.22 $\pm$ 1.72 collector channels) as compared with those lacking (5.11 $\pm$ 4.76 collector channels). No statistical significance was found ($p = 0.13$). Also, within the pool of frontally oriented samples, the variations in the number of signals within immunofluorescence-positive samples were likely to be smaller and more even than that found in the counterpart with no immunostaining.

In correspondence of the previously described interconnectivity between collector channels and supraciliary space at distal outflow pathways, immunofluorescence was found to be localized predominantly at the anterior outflow region only. No pattern of continuation in immunofluorescence toward supraciliary space was observed. Moreover, immunofluorescence shown in frontal orientation did not support continuous staining pattern in neighborhood among collector channels. No corresponding similarity or correlation between the Trichrome-stained and immunofluorescence samples was found in this study.

Discussion

In this study, visible collector channel ostia in frontal orientation of normal human eyes were shown to be mostly distributed at inferior nasal quadrant, at which these collector channels were interestingly displayed with different morphological appearance. Alpha-smooth muscle actin-specific immunofluorescence revealed to have more positive staining at CC ostia in radial perspective than that in frontal counterpart.

4.1. Morphological and Mechanical Observation of Collector Channel ostia and distribution pattern of α-Smooth Muscle Actin

Our results confirmed the presence of smooth muscle-like cells are in neighborhood of outer wall of Schlemm's canals and collector channel ostia, which appear to correspond with the findings by De Kater et al (1990 & 1992). These patent CC ostia were found to be predominantly present at inferior nasal region of the eyes in this study. It indicates that anatomical distribution of collector channels is not uniform but segmental. Nevertheless, a pilot study that reconstructed a panoramic view of anterior segment of human eyes using 3-dimensional micro-computed tomography (3-D micro-CT) displayed that collector channels were distributed randomly without any specific pattern in any quadrant in two human eyes (Hann et al., 2011). The discrepancy showing different localization patterns of collector channels in human eyes is highly variable, depending on multiple factors, including the thickness of sample slides used, parameters of voxel sizes by the 3-D micro-CT, as well as the nature of comparison. In our study, patent (unobstructed) collector channels were

identified and quantified by immunohistochemistry in 2-D perspective with the magnification factors ranging from 10x to 60x, whereas in Hann's study the distal outflow structure were prepared by both immersion-fixed and perfusion-fixed techniques and processed by 3-D imaging technology. Factors of magnification in the light microscopy, however, were not provided except the dimension of voxel scans (2 μm and 5 μm) in the 3-D volumetric analysis. Due to the different parameters used in the studies, the discrepancy of the distribution of CC ostia cannot be fully compared.

Anatomical distribution of collector channels is closely related to its functional characteristics in regulating the aqueous outflow pattern. Hann et al. (2009) found that increased level of fluorescent beads in pigmented region of trabecular meshwork adjacent to collector channels were more likely to concentrate in nasal and inferior regions. It suggests that preferential routes for outflow are likely to exist in distal outflow pathways. Similarly, a tracer study using cationized ferritin that binds to negatively charged membrane surfaces has shown that tracer diffusion pattern appeared to be more segmental in glaucomatous human eyes (De Kater et al., 1989).

Although evidence of segmental outflow pattern in human eyes has been reported, the exact mechanism of how aqueous outflow is governed segmentally still remains to be elucidated. Several factors have been considered in understanding the mechanisms of why increased fluid outflow occurs in these particular areas. We postulated that preferential outflow occurs either as 'active, selective outflow' mechanism, or 'passive, non-discriminatory filtering' consequence. Our result displayed that the distribution of both continuous and scattered

bead-like α-smooth muscle actin cells found adjacent to collector channels may play a role in modulating the junctions between the outer wall of Schlemm's canals and collector channel ostia. Extending from the Schlemm's canals, orifices of collector channels surrounded by these α-smooth muscle actin cells are likely to act as 'contractile valves', resulting in expansion of area under collector channels. In the study by Chen et al. (2007), α-smooth muscle actin expression upregulated by TGF-β1 were shown to enhance cellular traction force in myofibroblasts. Similarly, over two-third of human trabecular meshwork cells were reported having stress fiber expressions with positive staining for α-smooth muscle actin (Tamm et al., 1996). These results suggest that the outflow mechanism may actively result from a "seesaw" effect of contractile activity of α-smooth muscle actin in the neighborhood of trabecular meshwork, resulting in constant remodeling action of stress fibers. Extending this idea to the distal portion of the outflow structures, however, the biomechanical relationship between α-smooth muscle actin and Schlemm's canals and collector channels has not yet been determined. If α-smooth muscle actin were involved in regulating contractility of outer wall of Schlemm's canals and the adjacent collector channel ostia, it may help explore the possibility that α-smooth muscle actin may indeed play a role as an additional "gatekeeper" of outflow resistance at distal outflow region. Nevertheless, evidence in support of the role of smooth muscle actin at Schlemm's canals and collector channel ostia still remain inconclusive. An earlier study by Gipson & Anderson (1982) first reported that, in human eyes, bundles of "smooth muscle-like" actin filaments are found at the outer walls of Schlemm's canal, yet they were not associated with collector channels. Conversely, Hamanaka et al. (1997) found that, in cynomologus monkey eyes, endothelial

cells of Schlemm's canals are vascular in origin, and the α-specific actin type were stained, not so much at outer wall of Schlemm's canal, yet more located at the deep sclera adjacent to supraciliary space. However, the study by McMenamin and Lee (1982) indicated that, in a sample of 200 sections obtained from 20 pig tailed Macaque eyes using thin sections of 1-2 μm for light microscopy, collector channels are in continuity with Schlemm's canals in 35% of cases only. In other words, structural discontinuity exists between Schlemm's canal and collector channels in pig tailed Macaque, even observed at thin sample sections. Despite the variations of species types, it generally suggests that α-smooth muscle actin may or may not be present and continuous throughout the distal outflow route, and they may have different morphologies and functionalities depending on its location. .

In parallel with the postulated active outflow mechanism, the idea of pressure-dependent passive regulation of aqueous outflow may also be involved. In principle, pressure differential is required for fluid flow in all aspects. Among all aqueous outflow routes, areas near collector channel ostia generally have the greatest pressure differential up to 6 mmHg, as compared with that of 2-3 mmHg found between trabecular meshwork and Schlemm's canal (Johnson & Kamm, 1983). Using a mathematical flow model, aqueous outflow was found to be influenced by shear stresses at endothelial cells of Schlemm's canal. Outflow was found to reach its maximum near collector channel ostia, which resulted in mechanical changes in filamentous actin (F-actin) architecture (Ethier et al, 2004). As a result of the increased pressure difference and structural adaptation under collector channels, it may potentially allow expansion of JCT regions and, therefore, decreased distal outflow resistance. While collector channel ostia were found to have maximal rate of aqueous

outflow, it is also the most frequent site of collapse among all species, including human, bovine, and monkey eyes. In the model of *Macaca nemestrina* (McMenamin & Lee, 1982), numerous collagenous cords and septae in Schlemm's canals are present to favor aqueous drainage in order to maintain regional patency of the canals.

4.2. Distribution Patterns of Collector Channels & Factors of Variability

Earlier studies revealed similar findings that collector channels were irregularly distributed around the circumference of the eye, in which the quantities of collector channels are variable among different studies. Dvorak-Theobald reported that 24 to 31 collector channels were found in immersion-fixed human eyes, with a tendency of increased number of collector channels at the inferior quadrant (Dvorak-Theobald, 1955). In current study, despite the raw preferential localization of collector channels at inferior nasal quadrant, the overall count of collector channels among all quadrants and the associated smooth muscle-like cells found to be scarcer than those found in previous studies and they were not shown statistically different in any quadrant. We think that such discrepancy is likely due to the coarse cutting technique. Raw tissue sections were manually cut solely by gross observation in both radial and frontal orientations. Ideally, they should be cut at a right angle perpendicular to the surface (regardless of orientations) in order to maintain the best possible anatomy. Any oblique deviation of the cutting angle, as little as one micron, may result in disrupting or underestimating the count and the volume of distal collector channel ostia. It is likely that our raw samples could be grossly cut in a miniscule oblique angle, and thus the

overall count of collector channel ostia might be undermined. Moreover, the planes of sectioning obtained in our study simply represented a small specific portion of each sample. It might not truly reflect the whole architecture of collector channels if the cutting angle has already been slanted. Some of the peripheral structures might also be left out as well. Since not all sectioned slides were sequentially included due to wrinkling or torn structures, the observed structures might not fully appreciate the three-dimensional variations of collector channel ostia.

In parallel with the pilot mice study conducted in our research group in which frontal reconstruction of collector channel ostia in mice eyes was attempted as a blueprint and collector channels were revealed to be visible in the full panoramic view. There were approximately 30-40 collector channels found using a Z-stacking technique with ImageJ. It is a digital image processing technique in which a series of images of collector channel ostia taken at different focal distances were combined to appreciate the depth of field as well as the overall structural variation at depth. It is an important discovery, if present, because not all collector channel ostia develop in the same level of depth and some collector channels may actually be embedded which can only be revealed by Z-stacking. In this study, we have also attempted to view the presence and development of collector channel ostia in human eyes by the ImageJ software. However, the numbers of complete collector channel ostia collected in multi-sectoral planes found in human eyes were much varied from that found in the mice pilot model. In addition to the potential contributing factors listed previously, such as deviated angle of sectioning, or arbitrary section viewing within the whole structure, we think that thickness of sections may also be one of the key limitations. The samples in this

study were limited to its thinnest as 6 μm in paraffin sections whereas the samples in the mice model were made to be 1 μm in plastic sections. Few other studies also utilized plastic sections of 1-2 μm for 3-dimensional imaging (Hann et al, 2011; Kagemann et al, 2010). The six-fold difference in sample thickness used can be understood in that whole mice eyes (3.32 mm diameter measured from posterior surface of cornea to the optic nerve; Remtulla & Hallet. 1985) are much smaller than human eyes (28.0 mm diameter; Oyster, The Human Eye. 1999). Smaller eye size would be advantaged for the thinner sectioning under microtome, which, in turn, yield better image quality in finer details for which can be missed out in thicker slides. We now understood that sample thickness in human eyes as compared to that of mice eyes (6 vs 1 μm) may explain the discrepancy in quantifying collector channel ostia in human eyes, for which the number of collector channel ostia could have been underestimated in the coarse thickness measurement. Further modification of the protocol in optimizing the section thickness in human eyes would enable more accurate in-depth analysis of the distal outflow structures.

4.3. Factors governing Antibody Immunofluorescence

Positive immunofluorescence staining of α-smooth muscle actin in our study was found to be more spatially distinct in radial than in frontal sections. Although the technique of frontal sectioning have been previously adopted to examine giant vacuoles (Parc et al., 2000), herniation of inner wall and JCT into collector channel ostia, as well as changes in the effective filtration area of aqueous humor in response to IOP increase (Battista et al., 2008),

it is the first attempt used in this study to investigate the morphological characteristics of α-smooth muscle actin in distal outflow region in human eyes. In parallel with the studies by De Kater el al (1990 & 1992), where location of alpha and filamentous isoforms of smooth muscle actin (F-actin) were only examined in radial sections, our studies also characterized that the fusiform-like immunofluorescent patterns were located along the margin of the outer wall of Schlemm's canal, accompanied with trace distribution of fluorescent signals at the entrance of collector channel ostia. Similarly, our data in frontal view also revealed the presence, yet significantly less consistent immunofluorescent expression of α-smooth muscle actin, particularly at the neighborhood of collector channel ostia. Positive signals of α-smooth muscle actin were found to be present in some regions of collector channel ostia, yet not the others. Several possibilities are considered to account for the findings. First, it is likely that the exposure wavelengths of antigen-antibody binding were different between radial and frontal sections. Typically, anti-α smooth muscle actin antibody is in conjugation at a ratio of 6 moles of fluorescein to 1 mole of antibody. Signal of conjugation with the secondary antibody (Fluoro 488 goat anti-mouse IgG) appears to be at maximal excitation at wavelength of 488 nm and maximal emission at wavelength of 519 nm (obtained from Invitrogen Data sheet - Specification). In order to maximize the intensity of fluorescence signals, we ensured that the fluorescence filter setup of fluorescence microscopy is in sync with that elicited by the reagents. Meanwhile, due to high specificity of covalent, time-lapsed interactions between fluorophores, samples were treated with antibodies in dark condition and they were always covered up with aluminum foil immediately after the procedure. It was intended to minimize photobleaching, which occurs when fluorophores

loses the ability to fluoresce upon photo-induced destruction. Moreover, the discrepancy of fluorescence intensity may also be attributable to miniscule deviation of tissue sectioning angle; only partial conjugation of antibodies at the area of fluorescence exposure due to structural alteration of collector channel ostia; functional variations in the uptake of fluorescence molecules, etc. Moreover, the discrepancy of fluorescence intensity for α-smooth muscle actin between radial and frontal perspectives is unlikely due to changes of IOP gradients since all of our samples are normal, healthy human eyes and the structures had not been altered by means of IOP elevation. Rather, the heterogeneity of fluorescence patterns is more likely to be dependent on the intrinsic factors or interactions among neighboring cellular changes, or combination of both factors, at the distal outflow structures.

4.4. Roles of Transforming Growth Factor Beta-2 (TGF-β2) in α-smooth muscle actin cells

Myofibroblast-specific α-smooth muscle actin has also been implicated for its dynamic relationships with multifaceted growth factors for fibroblast differentiation, including tissue growth factor-β (TGF-β). In general, TGF-β is a potent cytokine involved in general wound healing and fibrosis (Roberts et al., 2003) and extracellular matrix (ECM) remodeling (Gabbiani, 2003; Tripathi et al., 1994). Upregulation of TGF-β1 was shown to enhance cell traction force in myofibroblasts, particularly α-smooth muscle actin (Chen et al., 2007; Tamm et al., 1996), possibly leading to geometric reorganization between inner and outer

wall of TM cells and, thus the whole actomyosin system of the outflow pathway (Tian et al., 2000).

Increased level of TGF-β2 has been found in aqueous humor in nearly 50% of eyes with POAG (Tripathi et al., 1994; Picht et al., 2001). In vitro, increased production of TGF-β2 by trabecular cells in glaucomatous eyes induced excess deposition of extracellular matrix (ECM) components in trabecular meshwork (Cao et al., 2002), glaucomatous optic nerve head astrocytes (Fuchshofer et al., 2005), as well as apoptosis of trabecular meshwork cells (Cao et al., 2004). It, in turn, resulted in decreased outflow facility, as shown in experimental perfusion models in human eyes (Gottanka et al., 2004) and rodent eyes (Shepard et al., 2010). Despite the active production of TGF-β in aqueous humor in glaucomatous eyes, it is still intriguing about why α-smooth muscle actin expression was shown to decline over time with age and in POAG in dogs and human (Hassel et al., 2007; Flögel et al., 1992). It suggests that the relationship between TGF-β and α-smooth muscle actin may be understood as being more 'mosaic' than 'static'. Han et al. (2011) indicated that extracellular matrix elasticity could be a key factor in modulation of TGF-β signaling cascade. In view of the contractile property of α-smooth muscle actin, it appeared that the regulation is more in a fluid-like 'mechano-sensitive' manner rather than a strict 'contraction-relaxation' relationship (Wang et al., 2006). Nevertheless, further study is to be warranted to further understand whether TGF-β directly increases contractile activity of α-smooth muscle actin cells, which results in further contraction in aqueous outflow pathway in glaucoma.

In addition to the variants of TGF-β, chemokines such as TNF-α has also been linked to the dynamics of trabecular metalloproteinase expression in POAG (Alexander et al., 1998 & 2003). Elevated level of TNF-α was evident in aqueous humor of glaucomatous human eyes (Sawada et al., 2010) and glaucoma-related optic neuropathy (Huang et al., 2010). The presence of TNF-α was reported to be more often found during the inflammatory phase of wound healing (Singer & Clark. 1999). These chemotactic cytokines were also evident to be constitutively secreted in cultured human TM cells (Shifera et al., 2010). As a result, interplay of these cytokinic mediators are not surprisingly linked to genotypic and/or phenotypic changes of α-smooth muscle mRNA expression. Goldberg et al. (2007) displayed that TGF-β and TNF-α, each individually, increased and decreased α-smooth muscle actin expression, respectively. In the same study, TNF-α was found to suppress TGF-β1-driven Smad-3 phosphorylation, from which it relaxed contractile strength of α-smooth muscle actin lattices post-5-day of wound healing culture. Since the cytokines are present and are constantly released at TM region, it implies that, at the distal outflow region, contractility of α-smooth muscle actin can also be modulated via antagonistic effects between the two cytokines. This may decrease the tensile strength of α-smooth muscle actin in the vicinity of collector channels, which further triggers mechanical realignment on extracellular matrix, and thus regulates outflow resistance. Several limitations are present in this part of our study. First, our study is mainly focus on morphological and spatial comparisons of α-smooth muscle actin near collector channels. Functional correlation between α-smooth muscle actin and cytokines, particularly in subject of regulation of aqueous outflow, was not covered and yet to be explored. Second, studies in investigation of cytokinic activities

mostly utilized human trabecular meshwork (HTM) cell culture in vitro or ex vivo (Bradley et al., 2000; Wordinger et al., 1998; Alexander et al., 1998), whereas our study was solely limited to comparisons of histological and immunohistochemical specimen. Such experimental protocol used in our study was valuable for indirect observation in post-treatment specimen, yet it might not fully appreciate how the cascade events of cytokines actually trigger contractile modulation of α-smooth muscle actin, just as shown in cell-cultured studies.

4.5. Patterns of Interconnectivity between Schlemm's canal and Supraciliary Space

Our results demonstrated the presence, yet inconsistent pattern, of potential interconnectivity among adjacent collector channels in both radial and frontal orientations. Although it currently still demands more substantial framework of how neighboring collector channels are indeed developed into cross-networking, knowledge of architectural anastomosis becomes increasingly popular and important in understanding the functional aspects of distal outflow drainage pathway. Prior to the investigation of arteriovenous anastomosis, a study by Hamanaka et al. (1992) attempted to explore the embryological development of Schlemm's canals and collector channels. It indicated that collector channels were likely to be derived from a vascular origin and aqueous humor was actually in mixture of blood within the sclera, which was drained into an episcleral venous plexus, posterior to the conventional corneoscleral route of outflow. Despite its controversy, arteriovenous anastomosis was

unlikely to be a result of pressure-induced phenomenon, yet more likely to be involved at the beginning of embryological stage of the distal outflow pathway.

Results of our study reflected discontinuous and inconsistent staining pattern between Schlemm's canal and supraciliary space locations. It was possibly attributable to several factors. First, episcleral vasculatures of the primates in previous studies were mostly pre-treated with nitroprusside prior to plastic injection, whereas none of samples in our study were chemically pretreated with nitroprusside. This step is likely to be crucial for the complete and longer-lasting patency of arterial and venous vasculature as well as other passageways since nitroprussin (Nipruton) has long been reported for usage of vasodilation in ischemia-related heart failure (Modersohn, Urbaszek, 1980; Brown, 1980). Similar experimental usage of nitroprusside as resin cast were also applied for unveiling the architecture of episcleral microvasculature by scanning electron microscopy in the owl and cynomolgus monkey (Funk & Rohen, 1996). Therefore, the absence of vasodilator agent in the preparation of specimen might account for the collapse of the architecture that connected to the episcleral venous plexus, which resulted in incomplete and consistent opening of collector channels observed in our study. Indeed, a recent study by Zamora & Kiel (2010) revealed that episcleral venous pressure (EVP) showed responses to increased amount nitroprussin, a nitric oxide (NO) donor. Consistent with the role of vasoregulation, nitroprussin was evident in playing a role, not only in maintenance of the patency of distal collector channel ostia, but also for the regulation of EVP, and thus IOP changes. Moreover, our study utilized immunohistochemistry as the main tool for identifying and comparing the localization pattern of α-smooth muscle actin at distal outflow region. Despite the increased

viewing perspective of frontal orientation, it still merely represented a 2-dimensional plane. We did not use scanning electron microscopy (SEM) as what the previous studies did (Funk and Rohen, 1996; Selbach et al, 1998), in which SEM was optimized to display the 3-dimensional structural framework of arteriovenous connections of episcleral vessels in higher magnification and in greater details. In general, these limiting factors may explain the challenges of displaying full patency of collector channels from anterior corneoscleral location to the supraciliary space. Further investigation of the anatomical framework of anastomoses between collector channels and episcleral venous plexus remains to be elucidated, which may help deepen the understanding of the aqueous outflow mechanism.

5. Direction of Future Studies

i. Identify collector channel ostia using thinner sections.

The samples sectioned in our study were ideally aimed to display the coarse morphological features of collector channel ostia in both radial and coronal perspective. However, it was later realized that the tissue slides used in our study were indeed too thick in microscopic scale, in which 6-micron paraffin-embedded slides cannot fully unveil or appreciate the true morphological variations or patterns of CC ostia in human eyes. As evident in our study, some CC ostia bifurcated symmetrically whereas others manifested obliquely across the z-plane of section. If the tissue slides were sectioned to be as thin as 1-2 microns, just as that attempted in the mice model (unpublished yet), it may enable better morphological overview of CC ostia at all levels.

ii. Reexamination of Immunostaining of α-smooth muscle actin and determine its role in regulating aqueous outflow

While α-smooth muscle actin was shown to be evident near CC ostia in our study, the immunostaining patterns of α-smooth muscle actin were much scattered and inconsistent. It was most likely due to the physical limitation of thinning the sample sections, which resulted in underestimation of the number of CC ostia. If we could find more CC ostia with thinner sections and repeat immunofluorescence staining of α-smooth muscle actin, we expect that there may be an increased amount of neighboring α-smooth muscle actin to be unveiled and its distribution of immunostaining would be important for determining its potential role in regulation of aqueous outflow.

iii. Role comparison of α-smooth muscle actin between normal and POAG human eyes

If α-smooth muscle actin distribution could be found in normal human eyes, our next goal is to compare its distribution pattern between normal and POAG human eyes and determine whether there were any expression difference between the two groups. Since α-smooth muscle actin has been suggested to influence the cellular contractility and geometric arrangements at the aqueous outflow regions (Tian et al., 2000), increased expression of this specific myofibroblast cell type may play a role in elevation of aqueous outflow resistance in POAG eyes as well.

6. Conclusion

The presence of α-smooth muscle actin positive cells at the region of collector channels has gradually been observed as an alternate focus in understanding the functional regulation of distal outflow pattern. Our study revealed that the gross distribution patterns of collector channel ostia were predominant at inferior nasal quadrant in frontal perspective. Various morphological heterogeneities of collector channel ostia have also been evaluated for the first time. Meanwhile, antibody immunofluorescence pattern for α-smooth muscle actin in radial perspective was shown to be more statistically prominent than that found in frontal perspective. The spatial discrepancy between radial and frontal perspectives was more likely to be attributable to the variability of exposure sites for antigen-antibody binding, rather than external driving forces for tissue alternation. In addition, cytokines, TGF-β and TNF-α, have also previously been shown to play a role in modulating the contractility of α-smooth muscle actin, which is likely to implicate with aqueous outflow resistance. Furthermore, potential interconnectivity between distal CC ostia and supraciliary space and/or neighboring CC ostia may further broaden the knowledge of other linkages at the antero-posterior corneoscleral pathway. Future studies involving the association between contractile activity of α-smooth muscle actin and outflow facility may further deepen the understanding of biomechanical regulation of aqueous outflow, and thus decreasing outflow resistance.

Bibliography

Alexander JP, Acott TS. Involvement of the Erk-MAP kinase pathway in TNFalpha regulation of trabecular matrix metalloproteinases and TIMPs. Invest Ophthalmol Vis Sci. 2003 Jan;44(1):164-9.

Alexander JP, Samples JR, Acott TS. Growth factor and cytokine modulation of trabecular meshwork matrix metalloproteinase and TIMP expression. Curr Eye Res. 1998 Mar;17(3):276-85.

Allingham RR, de Kater AW, Ethier CR. Schlemm's canal and primary open angle glaucoma: correlation between Schlemm's canal dimensions and outflow facility. Exp Eye Res. 1996;62(1):101-9.

Battista SA, Lu Z, Hofmann S, Freddo TF, Overby D, Gong H. Reduction of the available area for aqueous humor outflow and increase in meshwork herniations into collector channels following acute IOP elevation in bovine eyes. Invest. Ophthalmol. Vis. Sci. 49,5346-5352.

Bill A, Svedbergh B. Scanning electron microscopic studies of the trabecular meshwork and the canal of Schlemm--an attempt to localize the main resistance to outflow of aqueous humor in man. Acta Ophthalmol (Copenh). 1972;50(3):295-320.

Brown MJ. Vasodilator drugs: systemic and regional considerations. Anaesth Intensive Care. 1980 Aug;8(3):310-317

Brown RW, Chirala R (1995) Utility of microwave-citrate antigen retrieval in diagnostic immunohistochemistry. Mod Pathol. 8(5):515-20.

Cao Y, Wei H, Zhang Y, Da B, Lu Y. Effect of transforming growth factor-beta(2) on extracellular matrix synthesis in bovine trabecular meshwork cells. Zhonghua Yan Ke Za Zhi. 2002 Jul;38(7):429-32.

Cao Y, Wei H, Da B, Huang Y. Effect of transforming growth factor-beta 2 on phagocytosis in cultured bovine trabecular meshwork cells. J Tongji Med Univ. 2001;21(4):318-20.

Chen J, Li H, SundarRaj N, Wang JH. Alpha-smooth muscle actin expression enhances cell traction force. Cell. Motil. Cytoskeleton. 2007 Apr;64(4):248-57.

Chi V, George KC. Immunohistochemistry: Paraffin Sections Using the Vectastain ABC Kit from Vector Labs. J Vis Exp. 2007; (8): 308.

Coroneo MT, Korbmacher C, Flögel C, Stiemer B, Lütjen-Drecoll E, Wiederholt M. Electrical and morphological evidence for heterogeneous populations of cultured bovine tracbecular meshwork cells. Exp Eye Res 1991;52:375-388.

De Kater AW, Shahsafaei A, Epstein DL. Localization of smooth muscle and nonmuscle actin isoforms in the human aqueous outflow pathway. Invest Ophthalmol Vis Sci 1992 Feb;33(2):424-9.

De Kater AW, Spurr-Michaud SJ, Gipson IK. Localization of smooth muscle myosin-containing cells in the aqueous outflow pathway. Invest Ophthalmol Vis Sci 1990;31:347-353.

Dvorak-Theobald G. Further studies on the canal of Schlemm: its anastomoses and anatomic relations. Am J Ophthalmol. 1955;39:65-89.

Fischer AH, Jacobson KA, Rose J, Zeller R. (2008) Hematoxylin and Eosin staining of tissue and cell sections. CSH Protoc. May 1; 2008.

Flögel C, Tamm E, Lütjen-Drecoll E. Different cell populations in bovine trabecular meshwork: An ultrastructural and immunocytochemical study. Exp Eye Res 1991;52:681-690.

Flögel C, Tamm E, Lütjen-Drecoll E, Stefani F. Age-related loss of a smooth muscle actin in normal and glaucomatous human trabecular meshwork of different age groups. J Glaucoma. 1992;1:165-173.

Flügel-Koch C, Ohlmann A, Fuchshofer R, Welge-Lüssen U, Tamm ER. Thrombospondin-1 in the trabecular meshwork: localization in normal and glaucomatous eyes, and induction by TGF-beta1 and dexamethasone in vitro. Exp Eye Res. 2004 Nov;79(5):649-63.

Fuchshofer R, Birke M, Welge-Lussen U, Kook D, Lütjen-Drecoll E. Transforming growth factor-beta 2 modulated extracellular matrix component expression in cultured human optic nerve head astrocytes. Invest Ophthalmol Vis Sci. 2005 Feb;46(2):568-78.

Funk RH, Rohen JW. Scanning electron microscopic study of episcleral arteriovenous anastomoses in the owl and cynomolgus monkey. Curr Eye Res. 1996 Mar;15(3):321-7.

Gipson IK, Anderson RA: Acdtin filaments in cells of human trabecular meshwork and Schlemm's canal. Invest Ophthalmol Vis Sci 1979;18:547-561.

Gottanka J, Chan D, Eichhorn M, Lütjen-Drecoll E, Ethier CR. Effects of TGF-beta2 in perfused human eyes. Invest Ophthalmol Vis Sci. 2004 Jan;45(1):153-8.

Grant WM. Clinical measurements of aqueous outflow. Am J Ophthalmol. 1951;34:1603-1605.

Grant WM. Experimental aqueous perfusion in enucleated human eyes. Arch Ophthalmol. 1963;69:783-801.

Grant WM. Further studies on facility of flow through the trabecular meshwork. AMA Arch Ophthalmol. 1958;60:523-533

Grierson I, Millar L, De Yong J, Day J, McKechnie NM, Hitchins C, Boulton M. Investigations of cytoskeletal elements in cultured bovine meshwork cells. Invest Ophthalmol Vis Sci 1986;27:1318-1330.

Hamanaka T, Bill A, Ichinohasama R, Ishida T. Aspects of the development of Schlemm's canal. Exp Eye Res. 1992 Sep;55(3):479-88.

Hamanaka T, Thornell LE, Bill A. Cytoskeleton and tissue origin in the anterior cynomolgus monkey eye. Jpn J Ophthalmol. 1997 May-Jun;41(3):138-49.

Han H, Wecker T, Grehn F, Schlunck G. Elasticity-dependent modulation of TGF-β responses in human trabecular meshwork cells. Invest Ophthalmol Vis Sci. 2011 May 2;52(6):2889-96. doi: 10.1167/iovs.10-6640.

Hann CR, Bentley, MD, Vercnocke A, Ritman EL, Fautsch MP. Imaging the Human Aqueous Humor Outflow Pathway in Human Eyes by Three Dimensional Micro-Computed Tomography (3D micro-CDT). Exp Eye Res. 2011 February;92(2):104-111

Hassel B, Samuelson DA, Lewis PA, Gelatt KN. Immunocytochemical localization of smooth muscle actin-containing cells in the trabecular meshwork of glaucomatous and nonglaucomatous dogs. Vet Ophthalmol. 2007 Nov-Dec;10 Suppl 1:38-45.

Inoue T, Kawaji T, Inatani M, Kameda T, Yoshimura N, Tanihara H. Simultaneous increases in multiple proinflammatory cytokines in the aqueous humor in pseudophakic glaucomatous eyes. J Cataract Refract Surg. 2012 Aug;38(8):1389-97. doi: 10.1016/j.jcrs.2012.04.028.

Johnson, M. What controls aqueous humor outflow resistance? Exp. Eye Res. 2006;82:545-557.

Johnson M, Kamm RD. The role of Schlemm's canal in aqueous outflow from the human eye. Invest. Ophthalmol. Vis. Sci. 1983;24:320-25.

Johnson MC, Kamm RD. The role of Schelmm's canal in aqueous outflow from the human eye. Invest. Ophthalmol Vis Sci. 1983;24:320-325.

Johnstone MA, Grant WM. Pressure-dependent changes in structures of the aqueous outflow system of human and monkey eyes. Am. J. Ophthalmol. 1973;75:365-83.

Kagemann L, Wollstein G, Ishikawa H, Sigal IA, Folio LS, Xu J, Gong H, Schuman JS. 3D Visualization of Aqueous Humor Outflow Structures In-Situ in Humans. Exp Eye Res. 2011 September;93(3):308-315

Kanai K, Nunoya T, Shibuya K, Nakamura T, Tajima M (1998) Variations in effectiveness of antigen retrieval pretreatments for diagnostic immunohistochemistry. Res Vet Sci. 64(1):57-61.

Kass MA, Heuer DK, Higginbotham EJ, Johnson CA, Keltner JL, Miller JP, Parrish 2nd RK, Wilson MR, Gordon MO. The ocular hypertension treatment study: a randomized trial determines that topical ocular hypotensive medication delays or prevents the onset of primary open-angle glaucoma. Arch. Ophthalmol. 2002;120(6):701-13; discussion 829-30.

Klein BE, Klein R, Sponsel WE, Franke T, Cantor LB, Martone J, Menage MJ. Prevalence of glaucoma. The Beaver Dam Eye Study. Ophthalmology. 1992 Oct;99(10):1499-504

Knapper PA, Frabman AI, Bondareff W. A smooth muscle plexus associated with the aqueous outflow pathway of the rabbit eye. Anat. Rec. 1975;182:41-52.

Leber T. Studien über den flüssigkeitswechsel im auge. Albrecht Von Graefes Arch. Ophthalmol. 1873;19, 87-106

Leske MC, Connell AM, Schachat AP, Hyman L. The Barbados Eye Study. Prevalence of open angle glaucoma. Arch Ophthalmol. 1994 Jun;112(6):821-9

Mitchell P, Smith W, Attebo K, Healey PR. Prevalence of open angle glaucoma in Australia. The Blue Mountains Eye Study. Opthalmology. 1996 Oct;103(10):1661-9

Modersohn D, Urbaszek W. The use of sodium nitroprusside (Nipruton) in ischemia-related acute heart insufficiency. Z Gesamte Inn Med. 1980 Apr 1;35(7):289-96.

Oyster, The Human Eye, Raven Press 1999

Pavlin CJ, Sherar MD, Foster FS. Subsurface ultrasound microscopic imaging of the intact eye. Ophthalmology. 1990;97(2):244-50.

Pellicer EM, Sundblad A (1994) Antigen retrieval by microwave oven with buffer of citric acid. Medicina (B Aires). 54(2):129-32.

Picht G, Welge-Luessen U, Grehn F, Lütjen-Drecoll E. Transforming growth factor beta 2 levels in the aqueous humor in different types of glaucoma and the relation to filtering bleb development. Graefes Arch Clin Exp Ophthalmol. 2001 Mar;239(3):199-207.

Quigley HA, West SK, Rodriguez J, Munoz B, Klein R, Snyder R. The prevalence of glaucoma in a population-based study of Hispanic subjects: Proyecto VER. Arch Ophthalmol. 2001 Dec;119(12):1819-26

Remtulla S, Hallett PE. A schematic eye for the mouse, and comparisons with the rat. Vision Res. 1985;25(1):21-31.

Rosenquist R, Epstein D, Melamed S, Johnson M, Grant WM. Outflow resistance of enucleated human eyes at two different perfusion pressures and different extents of trabeculotomy. Current Eye Res. 1989;8:1233-40.

Ruiz-Ederra J, García M, Hernánadez M, Urcola H, Hernánadez-Barbáchano E, Araiz J, Vecino E. The pig eye as a novel model of glaucoma. Exp. Eye Res. 2005;81(5):561-9

Ruiz-Ederra J, Verkman AS. Mouse model of sustained elevation in intraocular pressure produced by episcleral vein occlusion. Exp. Eye Res. 2006;82:879-84.

Sakimoto G, Samejima M. Groups of smooth muscle cells lying close to the intrascleral collector channels located in the anterior chamber angle of the normal albino rabbits (I). 1977a. Act Soc. Ophthal. Jap. 81, 386-392.

Sakimoto G, Samejima M. Groups of smooth muscle cells lying close to the intrascleral collector channels located in the anterior chamber angle of the normal albino rabbits (II). 1977b. Act Soc. Ophthal. Jap. 81, 1006-012.

Sarunic MV, ASrani S, Izatt JA. Imaging the ocular anterior segment with real-time, full-range Fourier-domain optical coherence tomography. 2008;126(4):537-42.

Selbach JM, Rohen JW, Steuhl KP, Lütjen-Drecoll E. Angioarchitecture and innervation of the primate anterior episclera. Curr Eye Res. 2005 May;30(5):337-44

Shepard AR, Millar JC, Pang IH, Jacobson N, Wang WH, Clark AF. Adenoviral gene transfer of active human transforming growth factor-{beta}2 elevates intraocular pressure and reduces outflow facility in rodent eyes. Invest Ophthalmol Vis Sci. 2010 Apr;51(4):2067-76.

Shi SR, Chaiwun B, Young L, Cote RJ, Taylor CR. Antigen retrieval technique utilizing citrate buffer or urea solution for immunohistochemical demonstration of androgen receptor in formalin-fixed paraffin sections. J Histochem Cytochem. 1993 Nov;41(11):1599-604.

Sommer A. Intraocular pressure and glaucoma. Am J Ophthalmol. 1989 Feb 15;107(2):186-8

Sommer A. Epidemiology as it relates to screening for glaucoma. Surv Ophthalmol. 1989 Apr;33 Suppl:441-2; discussion 449-50

Tamm ER, Siegner A, Baur A, Lütjen-Drecoll E. Tranforming growth factor-beta 1 induces alpha-smooth muscle actin expression in cultured human and monkey trabecular meshwork. Exp Eye Res. 1996 Apr;62(4):389-97.

Toris CB, Gabelt BT, Kaufman PL. Update on the mechanism of action of topical prostaglandins for intraocular pressure reduction. Surv Ophthalmol. 2008;53 Suppl1:S107-20.

Tripathi RC, Li J, Chan WF, Tripathi BJ. Aqueous humor in glaucomatous eyes contains an increased level of TGF-beta 2. Exp Eye Res. 1994 Dec;59(6):723-7.

Tripathi RC, Chan WF, Li J, Tripathi BJ. Trabecular cells express the TGF-beta 2 gene and secrete the cytokine. Exp Eye Res. 1994 May;58(5):523-8.

Tripathi RC. Comparative physiology and anatomy of the aqueous outflow pathway. 1974. In: Davson H, Grahma Jr, L.T. (Eds), The Eye. Academic Press, New York, pp. 163-356.

Wang J, Zohar R, McCulloch CA. Multiple roles of alpha-smooth muscle actin in mechanotransduction. Exp Cell Res. 2006 Feb 1;312(3):205-14.

Worley A, Grimmer-Somers K. Risk factors for glaucoma: what do they really mean? Aust J Prim Health. 2011;17(3):233-9

Zamora DO, Kiel JW. Episcleral venous pressure responses to topical nitroprusside and N-Nitro-L-arginine methyl ester. Invest Ophthalmol Vis Sci. 2010 Mar;51(3):1614-20. doi: 10.1167/iovs.09-4530. Epub 2009 Oct 29.

Zhang Y, Toris C, Liu Y, Ye W, Gong H. Morphological and hydrodynamic correlates in monkey eyes with laser induced glaucoma. Exp. Eye Res. 2009;89:748-56.

Zhu J, Gong H. Morphological changes contributing to decreased outflow facility following acute IOP elevation in normal human eyes. Association for Research in Vision and Ophthalmology, 200. Annual Meeting. Fort Lauderdale, Florida USA: The Association for Research in Vision and Ophthalmology; 2008.

Zhu J, Ye W, Gong H. Development of a novel two color tracer perfusion technique for the hydrodynamic study of aqueous outflow in bovine eyes. Chin Med J (Engl). 2010 Mar 5;123(5):599-605.

Raw slide #	Aperio Image #	Orientation of Eye	Stained (S) or Unstained (US)	Quadrant	Clock-hour position (o'clock)	Total counts of patent distal collector channels in all clock-hour positions combined (x = counted as zero)
2	13732	OD	S	IT	7, 8	6
6	13752	OD	S	X	X	x
8	13751	OD	S	T	9	3
10	13749	OD	S	T/ ST	9, 11, 12	12
14	13747	OD	S	IN/ ST	5, 10	4
16	13745	OD	S	IN	5	2
18	13743	OD	S	IN/ ST	5, 9, 10	8
22	13739	OD	S	IN	5	3
24	13738	OD	S	IN	4	3
36	13736	OD	S	IN	2, 3, 4	10
36	13734	OD	S	IN	2, 3, 4	12
9	13750	OD	US	T/ ST	9, 11	6
11	13748	OD	US	I	6	2
15	13746	OD	US	IN	5, 7	3
17	13744	OD	US	IN/ ST	1, 5, 10	10
21	13742	OD	US	IN/ ST	1, 5, 9, 10	15
29	13737	OD	US	SN	2	3
35	13735	OD	US	N	2, 3, 4	7
37	13733	OD	US	N/ ST/ IT	3, 4, 5, 8 , 10	16
65OS (#48)	13723	OS	S	ST	1	1
65OS (#49)	13724	OS	S	ST/ IN	1, 7, 8	10
65OS (#55)	13725	OS	S	X	X	x
65OS (#57)	13726	OS	S	S	12	3
89OS (#15)	13727	OS	S	IN	10	3
89OS (#4)	13728	OS	S	X	X	x
89OS (#5)	13729	OS	S	N/ IN	7, 8, 9	11
89OS (#7)	13730	OS	S	N/ IN	7, 8, 9	9
89OS (#9)	13731	OS	S	N/ IN/ SN	7, 8 , 9 ,10	15
Total Avg						13

Table 1. Quadrant distribution of distal collector channels of human normal eyes in frontal sections. T = Temporal; S = Superior; I = Inferior; N =Nasal; ST = Superior temporal; IT = Inferior Temporal; SN = Superior nasal; IN = Inferior nasal; X = not indicated in raw data or not quantifiable due to poor quality of data. The total number of patent collector channels was summed up and rounded up to the whole integer based on the number of usable slides. Samples with <5 or 'x' collector channels were considered outliers and excluded from the final count.

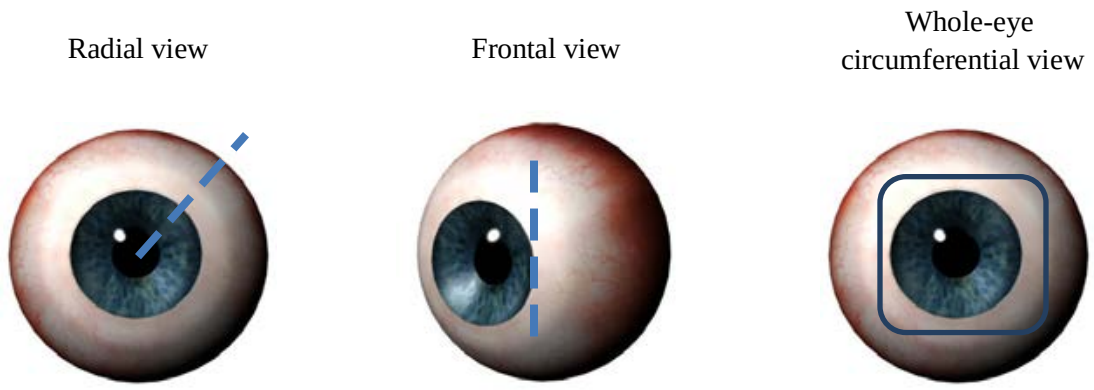


Figure 1. Dissection techniques of radial, frontal, and circumferential views. Radial section represented the plane of dissection perpendicular to limbus. Frontal section, on the other hand, showed the plane of dissection tangential to limbus. Circumferential section revealed panoramic, 360-degree, view of distal outflow structures in all quadrants.

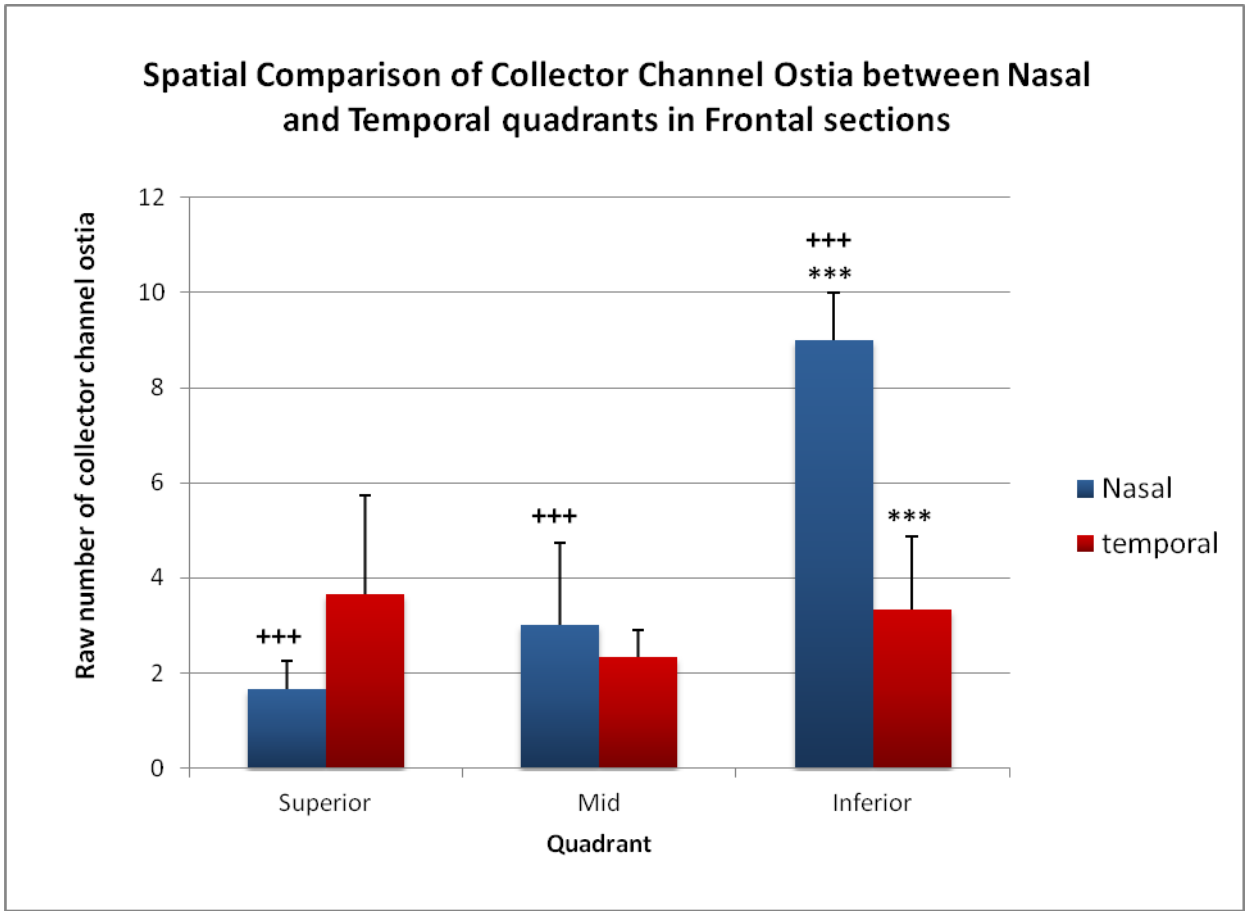


Figure 2. Spatial comparison of collector channel ostia between nasal and temporal quadrants in frontal sections (n=3). In perspective of nasal region only, the distribution of collector channel ostia among the superior, midsection, and inferior quadrants, collector channel ostia were predominantly localized at inferior quadrant with statistically significance (IN = 9.0; MN = 3.0; SN = 1.7; labeled as +++; one-way ANOVA, $p < 0.001$). However, collector channel ostia located at temporal regions among the same three quadrants did not show any statistical significance ($p = 0.569$). Within the inferior quadrant independently, collector channel ostia were shown to outnumber at nasal than temporal quadrant (IN = 9.0; IT = 3.3), and the spatial difference between the two regions was found to be statistically significant (labeled as ***; student T-test, $p < 0.01$). No other statistical significance was found between nasal and temporal regions within superior quadrant ($p = 0.561$) and midsection ($p = 0.184$), respectively. Legend: IN = inferiorly nasal; MN = midsection nasal; SN = superiorly nasal; IT = inferiorly temporal. Bars = S.D.

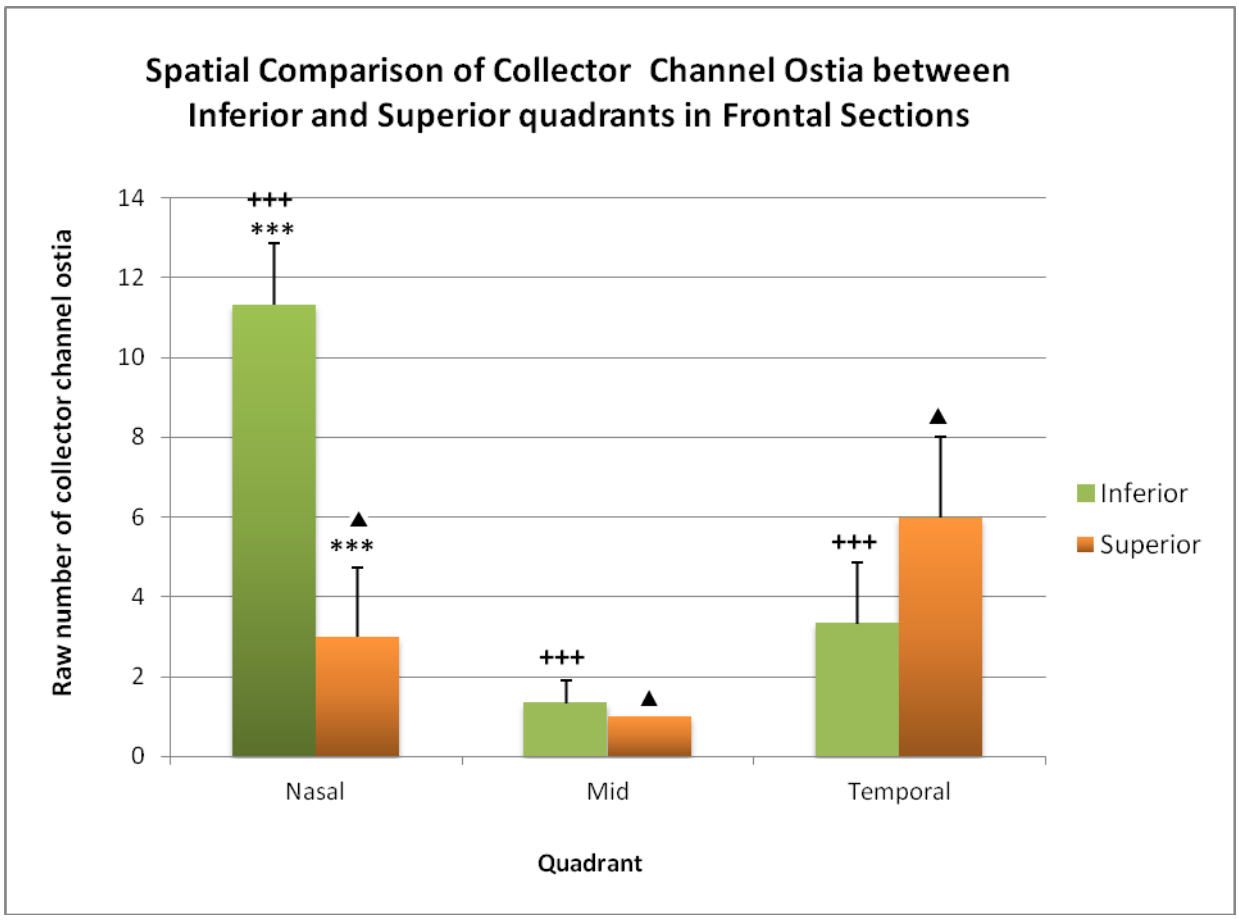


Figure 3. Spatial comparison of collector channel ostia between superior and inferior quadrants in frontal sections (n=3). In perspective of inferior region only, the distribution of collector channel ostia among nasal, midsection, and temporal quadrants were mostly localized at nasal quadrant and the difference among the three quadrants was statistically significant (NI = 11.3; MI = 1.3; TI = 3.3; labeled as +++; one-way ANOVA, $p < 0.0001$). In perspective of superior region among these three same quadrants, collector channel ostia were more likely to be found in temporal quadrant. Statistical significance was also shown among temporal, midsection, and nasal quadrants despite the difference appeared to be less obvious (TS = 6.0; MS = 1.0; TS = 3.0; labeled as ▲; $p < 0.05$). Within the nasal quadrant independently, the distribution of collector channel ostia were statistically greater at inferior than superior regions (NI = 11.3; NS = 3.0; labeled as ***; student T-test, $p < 0.005$). No other statistical significance was found between superior and inferior regions within midsection ($p = 0.374$) or temporal quadrant ($p = 0.14$). Legend: NI = nasally inferior; MI = midsection inferior; TI = temporally inferior; TS = temporally superior; MS = midsection superior; TS = temporally superior; NS = nasally superior). Bars = S.D.

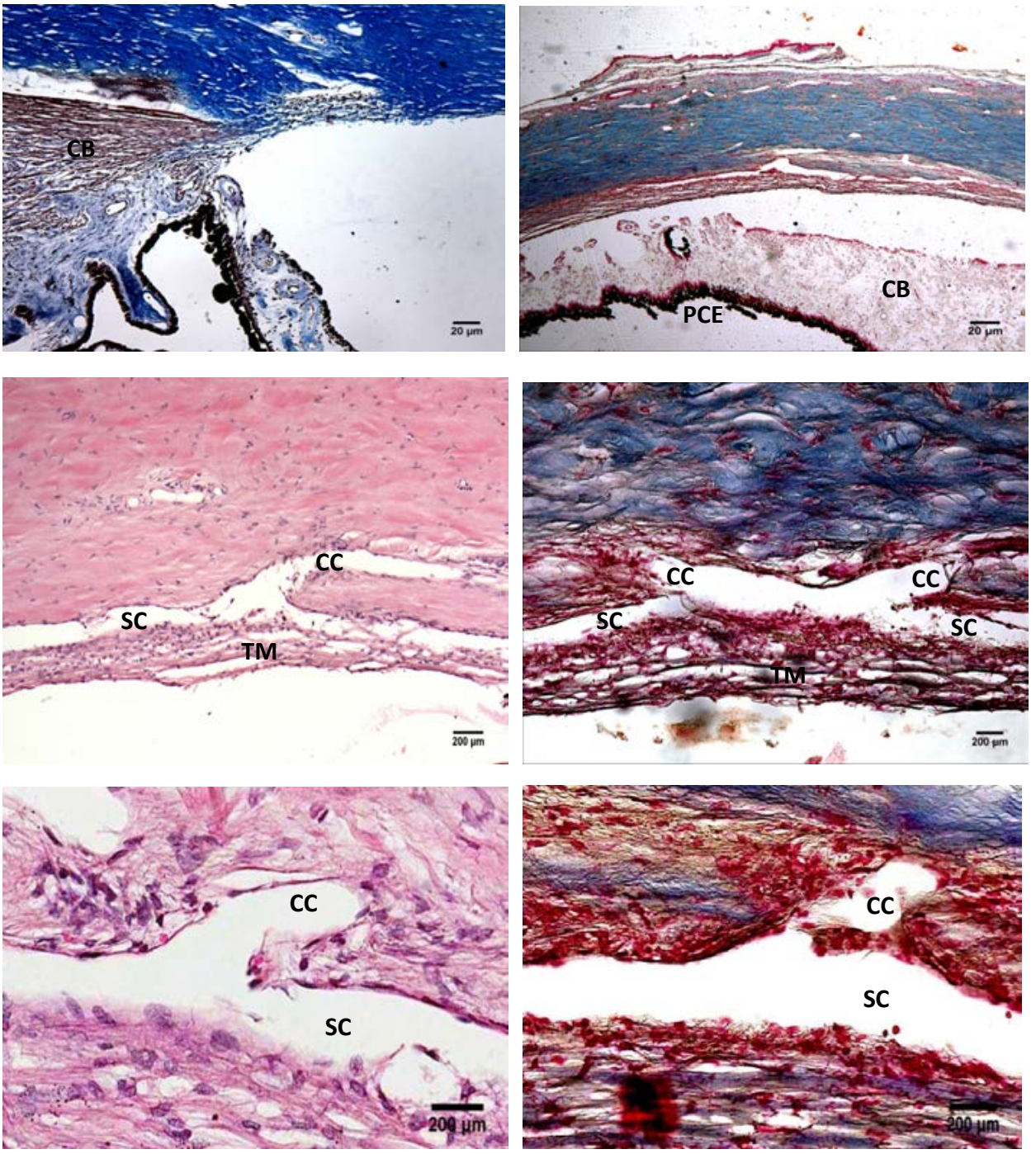


Figure 4. Comparison of Hematoxylin-Eosin (H&E) and Trichrome-Masson staining patterns in frontal orientation. H&E stains nucleic acid in blue or dark purple whereas cytoplasm and collagen fibers in pink. Trichrome solution stains collagen fibers in blue or dark purple while non-specific smooth muscle-like cells in red, which were shown to be localized along both inner and outer walls of Schlemm's canals, with evidence of extending distally at the "bottleneck" region toward collector channels. The results, however, did not show consistent findings of these smooth muscle-like cells. H&E stain were used as controls (C in 10x; E in 20x). Positive samples with Trichrome stain (A in radial in 4x; B in frontal in 4x; D in 10x; F in 20x). CB = Ciliary Body; PCE = Pigmented Ciliary Epithelium; TM = Trabecular meshwork; SC = Schlemm's canal; CC = Collector channel.

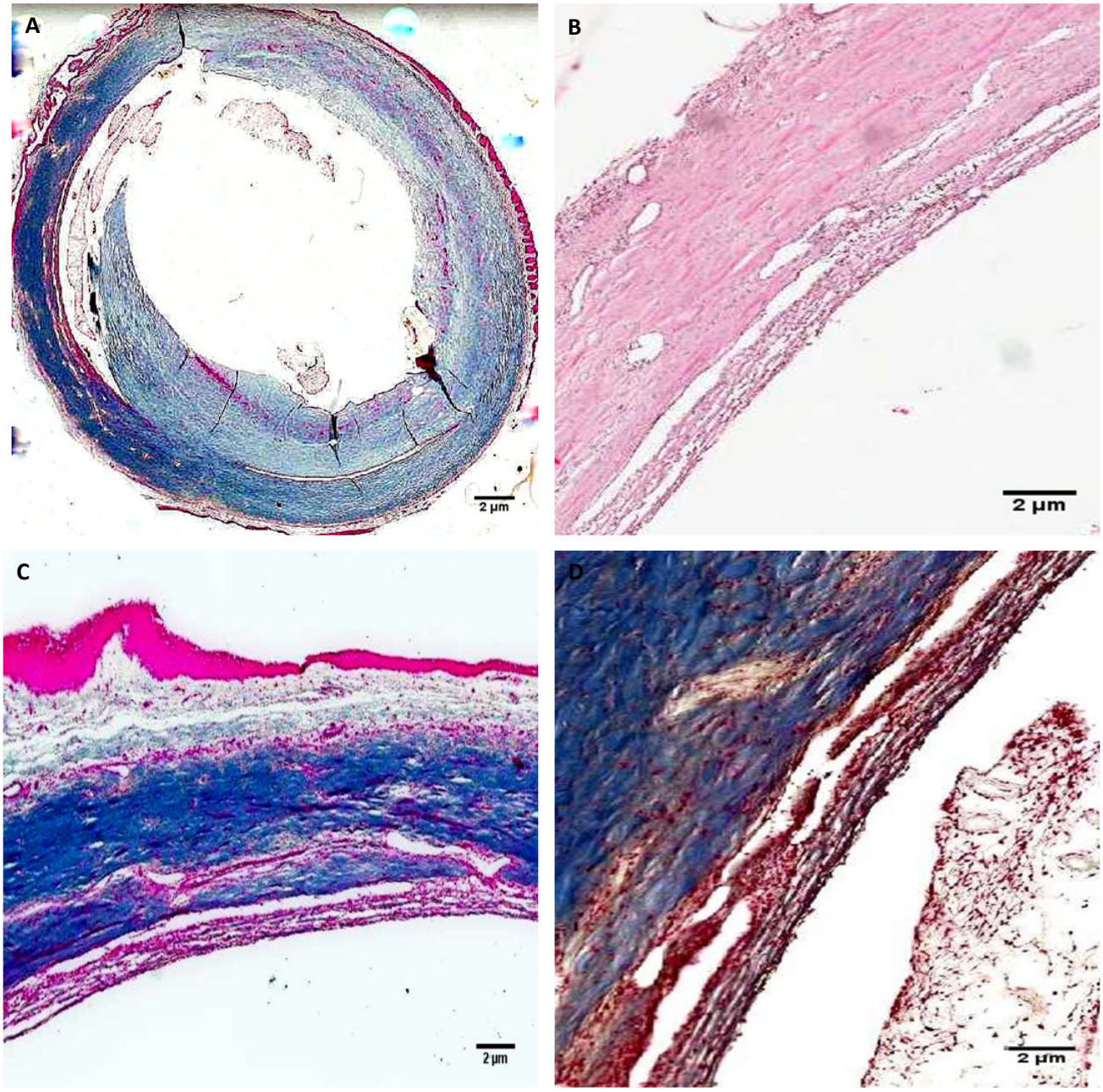


Figure 5. Interconnectivity of adjacent collector channels and episcleral venous plexus stained with Trichrome-Masson solution was illustrated in frontal view. A single circumferential section (A) of normal non-glaucomatous human eye (left eye shown here), displayed collector channels were preferentially localized in nasal quadrant with structural coalescence to neighboring collector channels (representative sample only). H&E stain was used as a control shown in (B). Collector channels in (C) budding out from Schlemm's canal was found to extend and connect to adjacent structures, potentially episcleral venous plexus . In (D), collector channels stained in Trichrome red was displayed as one of the morphological variations, of which the channels were fully developed with lateral extension, rather than "budding out" immaturely as shown in (C), before extending to adjacent structures. Fig. 4a in 2x; 4B & 4C in 5x; 4D in 10x.

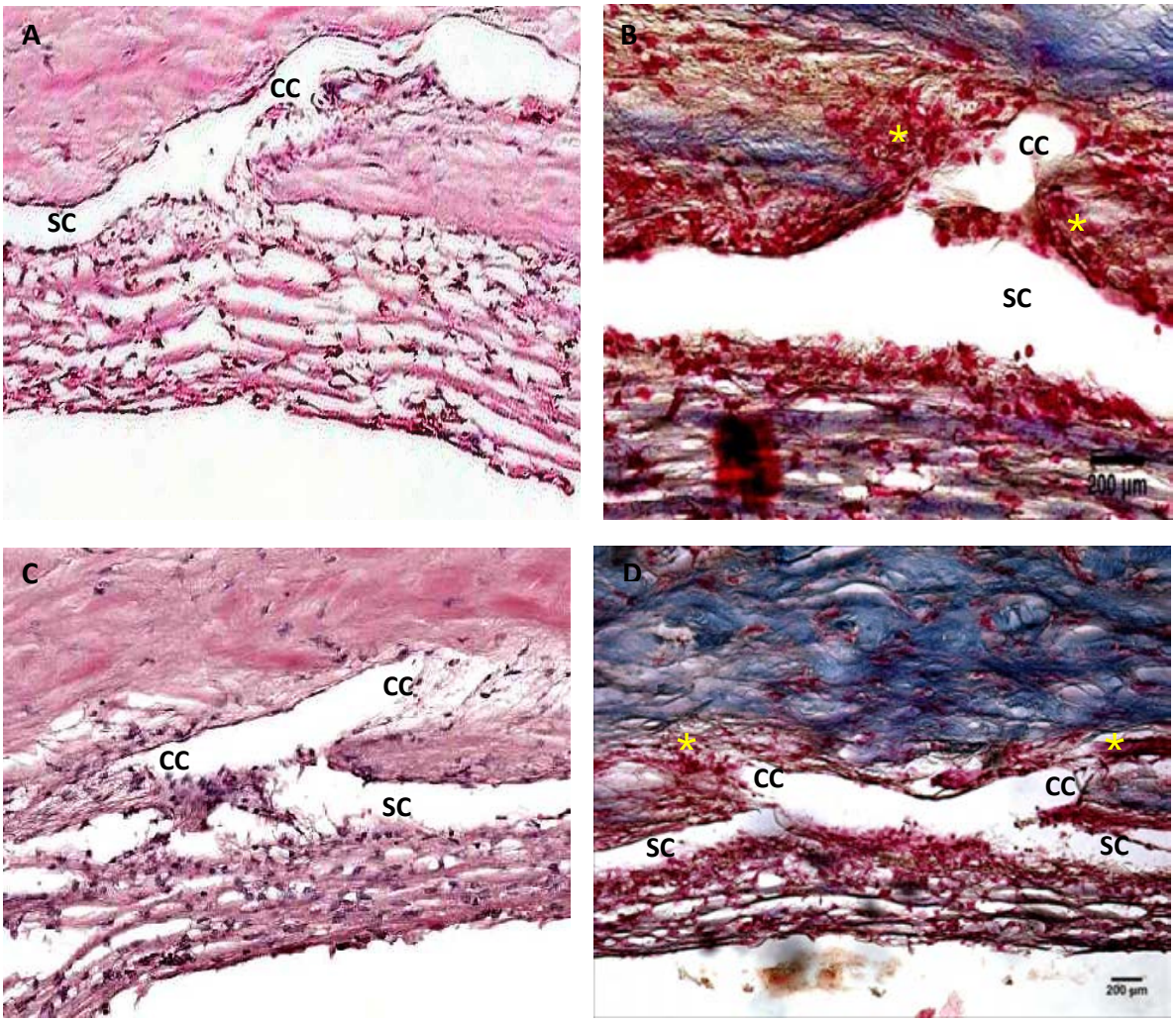


Figure 6. Morphological types of collector channel ostia observed in frontal perspective. Diagram A & C depicts H&E staining as the controls. Diagram B represents an oblique, unidirectional extension of CC ostia from the bottleneck region of Schlemm's canal. Diagram D reveals bidirectional budding of CC ostia in Y-shaped bifurcation. The extent and intensity of trichrome staining were shown to be more prominent for smooth muscle-like cells adjacent to the bottleneck opening of CC ostia (shown in asterisks). Diagram A to D all in 20x.

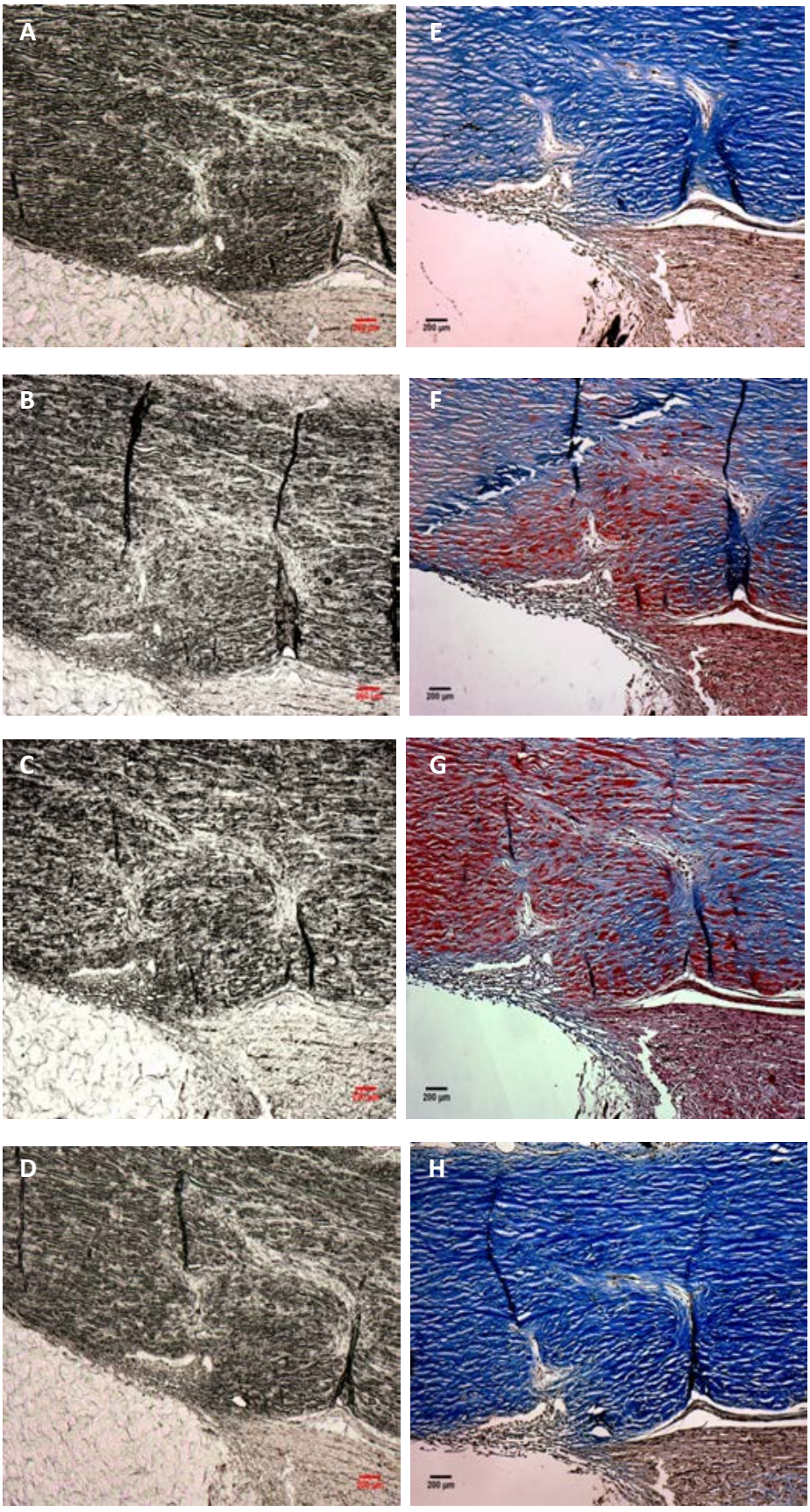


Figure 7. Comparison of interconnectivity between collector channels and supraciliary space in serial section of pre- and post-Trichrome-Masson staining. Pre-Trichrome samples showed distinct, well-demarcated collector channels developing from trabecular outflow region and extend posteriorly, seemingly to connect with supraciliary space (A to D). Post-Trichrome treated samples, however, could not confirm this interconnectivity between SC/CC and supracilairy space previously observed in our serial section data set (E to H).

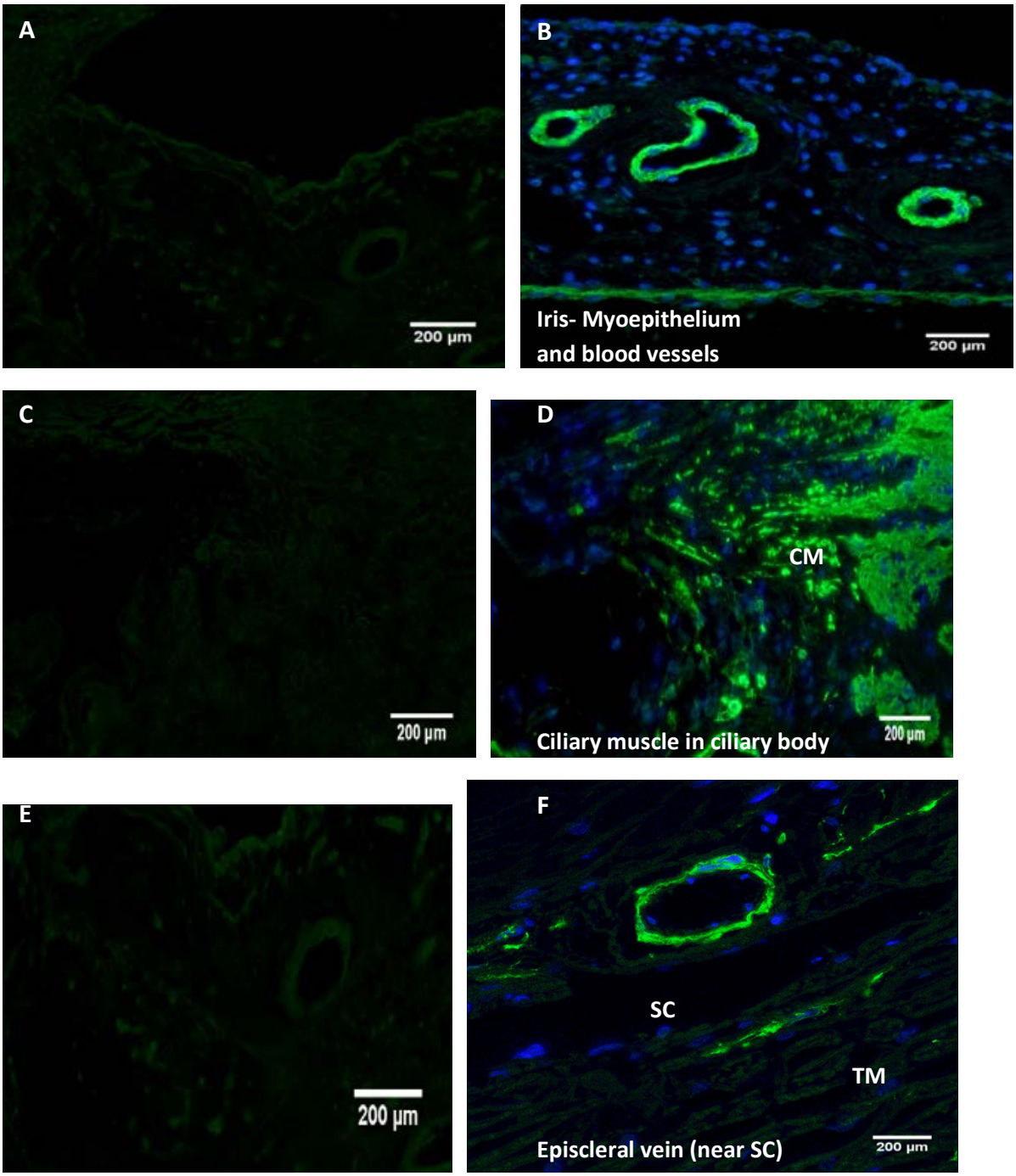


Figure 8. Indirect immunofluorescence staining for α-smooth muscle actin with monoclonal anti-mouse primary antibody (IgG2α; Sigma A2547) and secondary antibodies (Alexa Fluor 488 goat anti-mouse IgG (H+L); Invitrogen A11001) was demonstrated in various human ocular structures. Negative control (A, C, & E – all in 15x). Positive immunofluorescence staining of α-SM actin was seen in iris blood vessels and dilator muscle (B; 15x), ciliary muscles (D; 15x), and episcleral vein adjacent to the outer wall of Schlemm's canal (SC) and in the trabecular meshwork (arrow)(F; 40x) (green), Blue = DAPI (Life Technologies) for nucleus staining.

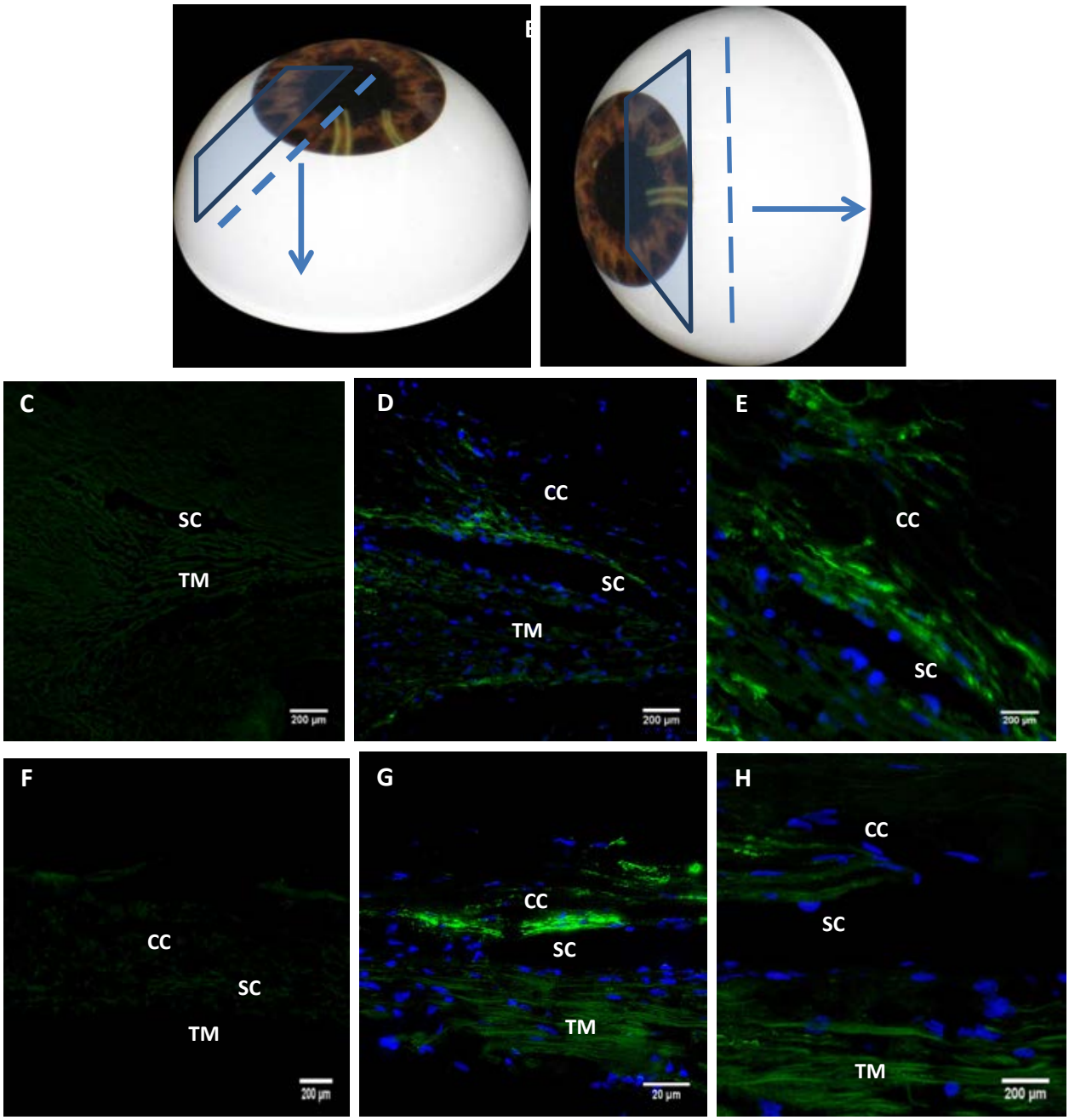


Figure 9. Distribution of immunofluorescence at regions of collector channels were shown in radial (A) and frontal (B) perspectives based on unique sectioning technique adopted previously (Battista et al, 2008). Sections in radial view (D & E) displayed positive antibody immunofluorescence for α-SM actin that were concentrated at specific regions, which was suggestive of preferential localization of α-SM actin at the junctions of outer wall of Schlemm's canal in pyramidal configuration toward collector channels (Fig. 8D; 20x), yet the staining pattern was sparsely found at distal region of collector channels (Fig. 8E; 40x). Negative controls in absence of monoclonal anti-mouse primary antibody were shown in Fig. 8C & 8F (10x). In view of frontal orientation, however, the intensity of immunostaining shown (G & H) appeared to be even much weaker and more scattered. Alpha-SM actin fibers seemed to align more at the 'bottleneck' before the bifurcation toward Y-shaped collector channels (Fig. 8G). In addition, the discontinuity of α-SM actin

presented as trace ‘punctate’ appearance was found only at the distal tip of collector channels rather than ‘satellite’ appearance, which was the first hypothesized configuration of α-SM actin, if existed at the distal outflow regions (Fig. 8H). Blue = nuclei stained with DAPI. TM = Trabecular meshwork; SC = Schlemn’s canal; CC = Collector channel

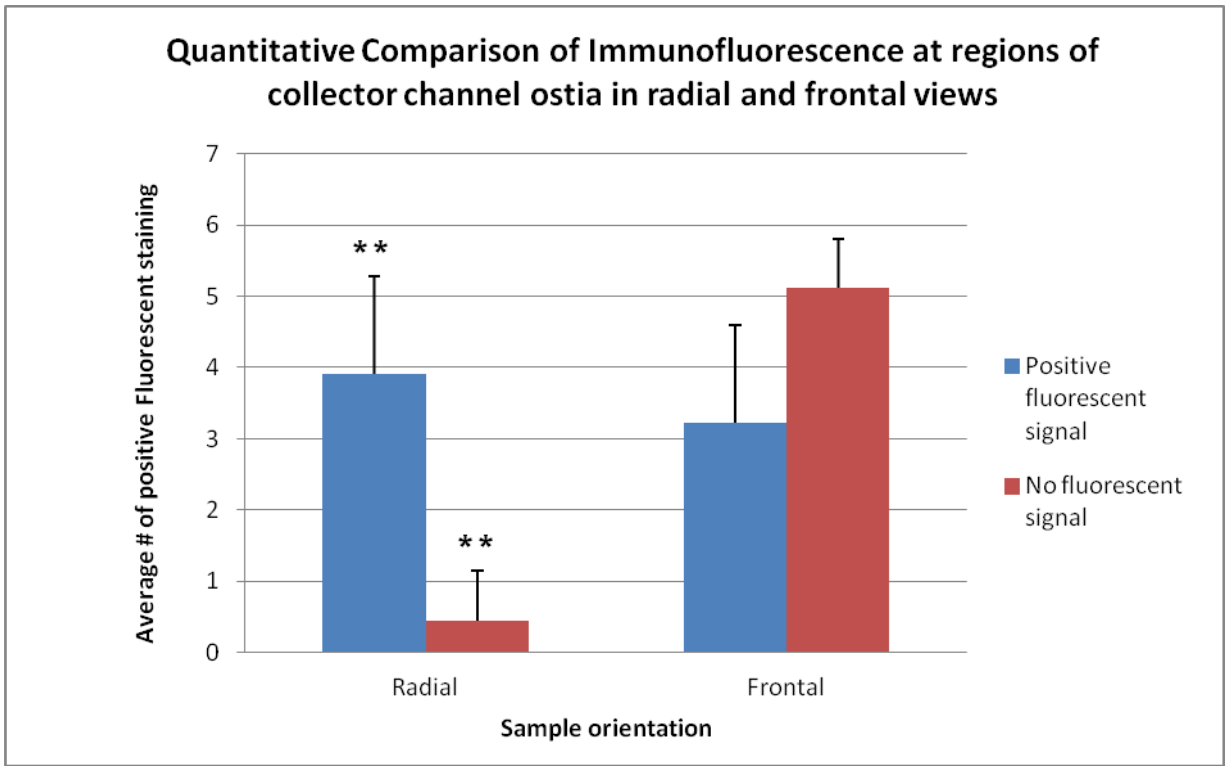


Figure 10. Quantitative Comparison of immunofluorescence at regions of collector channel ostia was observed in radial (n=4 after exclusion of two wrinkled and torn samples) and frontal (n=3) views, respectively. Immunofluorescence signals were shown to be more prominent in radial rather than frontal sections. In radially oriented samples, positive immunofluorescence signals depicting α-SM actin at distal collector channel region were observed to be more statistically significant than the CCs with no staining ($P < 0.0001$). However, in frontal view, no statistical significance was found between collector channels expressing positive fluorescence staining and those lacking staining ($p = 0.129$). Bars = S.D.